



SAPIENZA  
Università di Roma  
Facoltà di Scienze Matematiche Fisiche e Naturali

PhD Course in Cell and Developmental Biology

XXXII Cycle  
(A.A. 2018/2019)

**H3K9 methylation controls  
Fibro-Adipogenic Progenitors identity and skeletal  
muscle repair**

**PhD Student**  
Beatrice Biferali

**Supervisor**  
Dr. Chiara Mozzetta

**Coordinator**  
Prof. Giulia De Lorenzo

## INDEX

<b>Aim of the work</b>	<b>4</b>
<b>Summary</b>	<b>6</b>
<b>Sommario</b>	<b>7</b>
<b>Introduction</b>	<b>9</b>
<b>Results</b>	<b>14</b>
<b>G9a and GLP are enriched in FAPs</b>	<b>14</b>
<b>G9a/GLP silence the myogenic transcriptional program in FAPs</b>	<b>16</b>
<b>Prdm16 is a FAP-specific, nuclear lamina-enriched factor, that mediates H3K9me2 deposition at muscle-specific loci</b>	<b>19</b>
<b><i>In vivo</i> FAPs-specific ablation of Prdm16</b>	<b>24</b>
<b>Prdm16 preserves nuclear integrity and mediates H3K9me2-dependent tethering of muscle loci at the nuclear lamina</b>	<b>28</b>
<b>FAPs participate to skeletal myogenesis <i>in vivo</i> upon inhibition of H3K9 di-methylation</b>	<b>32</b>
<b>H3K9 KMTs accumulate in FAPs from degenerating dystrophic muscles</b>	<b>37</b>

<b>Discussion</b>	<b>39</b>
<b>Material and methods</b>	<b>42</b>
<b>References</b>	<b>59</b>
<b>Supplementary figures</b>	<b>68</b>
<b>Glossary</b>	<b>71</b>

## **Aim of the work**

The dual role of Fibro-Adipogenic Progenitors (FAPs), as either supportive of myogenesis in the early phases of regeneration or detrimental at later stages by causing fat and fibrosis deposition, makes them an attractive target for the development of pharmacological therapies aimed to improve regeneration, and to hinder fibro-adipogenic degeneration, of diseased muscles (Biferali et al., 2019). Therefore, the identification of the epigenetic players governing their phenotypical plasticity holds therapeutic potential. Chromatin modifying enzymes offer a repertoire of possible druggable targets. Among them, lysine methyltransferases (KMTs) are becoming increasingly studied thanks to their selectivity for defined histone residues and degree of methylation.

Preliminary evidence accumulated in our laboratory, and data from the literature, led us to hypothesize that Histone H3 lysine 9 (H3K9) KMTs might act as key stabilizing factors of FAPs-specific gene expression programs possibly regulating their myo-adipogenic switch.

Thus, the aim of my PhD project is to study the role of H3K9 methylation in FAPs lineage determination.

To this end, we first assessed expression of the major H3K9 KMTs, finding G9a and GLP to be particularly enriched in FAPs, as compared to muscle stem cells (MuSCs). To assess their functional role in mediating FAPs differentiation capacities, we performed G9a/GLP loss of function experiments coupled to transcriptional analysis and H3K9me2 chromatin immunoprecipitation studies. In an attempt to identify FAP-specific DNA-binding factors responsible of G9a/GLP chromatin recruitment, we focused on Prdm16 in light of previous data showing it interacts and recruits GLP at muscle-specific genomic regions in embryonic precursors (Ohno et al., 2013). Through different biochemical approaches, we

studied the functional interplay between Prdm16 and G9a/GLP in FAPs. Moreover, to define the functional role of Prdm16-dependant H3K9 methylation *in vivo*, we conditionally ablate it in FAPs generating Prdm16<sup>lox/lox</sup>:PDGFR $\alpha$ <sup>CreERT2/+</sup> double transgenic mice. We then assessed the impact of FAP-specific Prdm16 depletion in the overall muscle regeneration process and in FAPs fate determination.

Finally, by taking advantage of different murine models, comprising FAPs-specific reporter mice (PDGFR $\alpha$ -H2B:EGFP mice) and a FAP-specific lineage tracer (Osr1GCE/+;R26RmTmG/+ mice) (Vallecillo-Garcia et al., 2017; Stumm et al., 2018), we assessed the capacity of FAPs to participate to myogenesis *in vivo*, by treating them with the G9a/GLP specific inhibitor (A-366).

## Summary

Fibro-Adipogenic Progenitors (FAPs) are crucial regulators of muscle homeostasis as they possess the intrinsic ability to either support muscle regeneration or to contribute to fibro-adipogenic degeneration of dystrophic muscles. Therefore, the elucidation of the molecular mechanisms controlling their phenotypical plasticity holds therapeutic potential. Here we provide evidence that FAPs are particularly enriched in histone H3 lysine K9 methyltransferases (H3K9 KMTs), G9a, GLP and Prdm16. Our data indicate that H3K9 KMTs safeguard FAPs identity by repressing alternative transcriptional programs through deposition of H3K9 dimethylation (H3K9me2). Specifically, we show that Prdm16 controls G9a/GLP-mediated deposition of H3K9me2 at muscle-specific loci. Of note, we found Prdm16, G9a and GLP particularly enriched at the nuclear lamina (NL) of FAPs, suggesting they organize heterochromatin at the nuclear periphery to maintain the stable repression of genes encoding alternative developmental regulators. Accordingly, pharmacological inhibition or RNAi-mediated knock-down (KD) of H3K9 KMTs de-repress master myogenic genes in FAPs and induce the muscle differentiation program. Together, our findings reveal a FAPs-specific epigenetic axis important to control their identity. These findings are important especially for the possible therapeutic application to conceive strategies aimed to reprogram FAPs fate *in vivo* to prevent degeneration of diseased muscles.

## Sommario

I progenitori Fibro-Adipogenici (FAPs) sono una popolazione cellulare cruciale nel regolare l'omeostasi del muscolo scheletrico. I FAPs possiedono infatti un'intrinseca capacità di supportare la rigenerazione muscolare attraverso la produzione di fattori paracrini che promuovono il differenziamento delle cellule staminali muscolari, le cellule Satelliti (MuSCs); tuttavia possiedono la capacità di differenziare esse stesse in cellule fibrotiche e adipose, contribuendo alla degenerazione fibro-adipogenica del tessuto muscolare. Pertanto, comprendere i meccanismi molecolari che regolano questo fenotipo alternativo dei FAPs può avere importanti implicazioni terapeutiche proprio per il ruolo di questa popolazione cellulare nel mediare la rigenerazione e la degenerazione muscolare. In questo lavoro, evidenziamo che i FAPs esprimono livelli elevati di metiltrasferasi specifiche per la mono- e la dimetilazione della Lisina (K) 9 dell'istone H3 (H3K9 KMTs), quali G9a, GLP e Prdm16. I nostri dati indicano che questi enzimi salvaguardano l'identità dei FAPs reprimendo programmi trascrizionali alternativi attraverso la deposizione di H3K9me2. Nello specifico, dimostriamo che Prdm16 controlla la deposizione di H3K9me2 mediata da G9a/GLP a livello dei geni muscolo-specifici. Abbiamo inoltre evidenziato che Prdm16, G9a e GLP sono particolarmente arricchite alla lamina nucleare. Tale localizzazione ci suggerisce che queste metiltrasferasi possano organizzare l'eterocromatina alla periferia del nucleo in modo tale da mantenere la repressione stabile di quei geni responsabili dei programmi di differenziamento alternativo dei FAPs. Inoltre, l'inibizione farmacologica e il silenziamento, mediato da RNAi, delle KMT H3K9 è in grado di attivare i principali geni miogenici nei FAPs inducendo un'attivazione del programma di differenziamento muscolare. Nel complesso, i nostri dati rivelano

uno specifico controllo epigenetico che regola l'identità dei FAPs e mettono in evidenza il ruolo di questi enzimi come potenziali bersagli farmacologici per promuovere la riprogrammazione promiogenica dei FAP *in vivo*, prevenendo così la degenerazione e la perdita progressiva della funzione muscolare in muscoli affetti da patologie degenerative.

## Introduction

Skeletal muscle has a high, but non-inexhaustible, capacity to regenerate following injury. The regenerative potential of skeletal muscle relies primarily on Satellite Cells (MuSCs), the prototypical muscle stem cells, which reside in an anatomically defined stem cell niche beneath the basal lamina of myofibers. In resting muscles, they are normally present as quiescent progenitors. Upon muscle injury MuSCs enter the cell cycle and undergo several rounds of proliferation to expand the population suitable for differentiation to repair damaged myofibers and also to repopulate the reserve pool (Brack and Rando, 2012; Wang et al., 2013). Genetic approaches demonstrated the absolute requirement of MuSCs for an efficient skeletal muscle repair (Lepper et al., 2011; Murphy et al., 2011; Sambasivan et al., 2011), however their regenerative capacity depends on different cells present, or recruited, in the muscle regenerative niche (Wosczyzna and Rando, 2018). Among them, a population of interstitial mesenchymal stem cells, named Fibro-Adipogenic Progenitors (FAPs), has been recently demonstrated essential for long-term homeostatic maintenance and repair of skeletal muscle (Wosczyzna et al., 2019). FAPs have been defined as bi-potent muscle-resident progenitors capable to differentiate *in vitro* and *in vivo* in fibroblasts and adipocytes (Joe et al., 2010; Uezumi et al., 2010). In fact, during skeletal muscle regeneration, FAPs quickly proliferate and expand, prior to MuSCs, providing a transient favorable environment to promote, paracrinally, satellite cell-mediated regeneration (Heredia et al., 2013; Joe et al., 2010, Lemos et al., 2015; Lukjanenko et al., 2019, Mozzetta et al., 2013). Intriguingly, beyond their supportive role in muscle regeneration, FAPs have been shown to be the major source of fibroblasts and adipocytes in degenerating muscles (Kopinke et al., 2017; Mozzetta et al., 2013; Uezumi et al., 2010; Uezumi et al., 2011). When the

regeneration fails, as in dystrophic muscles at advanced stages of disease, these cells turn into fibro-adipocytes, being no longer able to promote myogenic potential of satellite cells and leading to gradual accumulation of fatty and fibrotic infiltrate within the muscle (Kopinke et al., 2017; Mozzetta et al., 2013; Uezumi et al., 2010; Uezumi et al., 2011). Recent studies have begun to elucidate the signaling pathways responsible of FAPs phenotypical plasticity in physiological and pathological conditions (Heredia et al., 2013; Kopinke et al., 2017; Lees-Shepard et al., 2018; Lemos et al., 2015), but the molecular events that govern their alternative phenotypes are still rather unexplored.

We recently unveiled a previously unappreciated plasticity of FAPs in response to regeneration cues (Mozzetta et al., 2013; Saccone et al., 2014) demonstrating that pharmacological manipulation of their epigenetic state, by inhibition of histone deacetylases (HDAC), unmask a latent myogenic potential (Saccone et al., 2014) and enhances their ability to promote differentiation of MuSCs in actively regenerating muscles (Mozzetta et al., 2013). Of note, HDACi are able to unmask a myogenic activity only in FAPs from actively regenerating muscles, such as those at early stages of Duchenne Muscular Dystrophy (DMD) progression (Saccone et al., 2014). By contrast, FAPs derived from degenerated dystrophic muscles are resistant to HDACi-mediated pro-myogenic activity, suggesting that their phenotypical plasticity is hindered by additional silencing mechanisms (Mozzetta et al., 2013; Saccone et al., 2014). Inhibition of HDACs and the consequent induction of histone hyperacetylation are generally accompanied by a global dispersion of H3K9 methylation (Taddei et al., 2001), thus suggesting that methyltransferases (KMTs) specific for H3K9 might be involved in the stable repression of the myogenic program in FAPs.

The best characterized H3K9 KMTs include SUV39 family members: SUV39h1, SETDB1, G9a and GLP (Mozzetta et al., 2015). KMT1A/SUV39h1 has been the most described in the context of skeletal muscle differentiation thus far. SUV39h1 is mainly responsible of H3K9 tri-methylation (H3K9me<sub>3</sub>) and it is involved in the permanent silencing of E2F-target genes in terminally differentiated myotubes (Ait-Si-Ali et al., 2004; Guasconi et al., 2010), and of differentiation genes in undifferentiated myoblasts (Mal, 2006; Zhang et al., 2002). SETDB1 has been shown to be required for adult muscle stem cells expansion following activation; and its re-localization from the nucleus to the cytoplasm, upon Wnt signalling activation, is necessary to allow muscle differentiation (Beyer et al., 2016). G9a and GLP, responsible for mono- and di-methylation of H3K9 (H3K9me<sub>1/2</sub>) (Shinkai and Tachibana, 2011), have been also implicated in the epigenetic regulation of muscle-specific program. In particular, G9a directly methylates MyoD (Ling et al., 2012a) and MEF2D (Choi et al., 2014) in proliferating myoblasts thus antagonizing their activity required to induce muscle genes transcription (Puri and Sartorelli, 2000). GLP has been instead identified as the H3K9 methyltransferase activity of the Prdm16 transcriptional complex (Ohno et al., 2013), a well-known potent inhibitor of muscle differentiation (Seale et al., 2008). GLP cooperates with Prdm16 complex, to silence the muscle-specific transcriptional program of a population of myogenic Myf5<sup>+</sup> progenitors, thus driving their lineage switch towards a brown-fat phenotype (Ohno et al., 2013). Prdm16 regulates the activity of different stem cells populations, including hematopoietic, neural and intestinal stem cells (Aguilo et al., 2011; Chuikov et al., 2010; Inoue et al., 2017; Shimada et al., 2017; Stine et al., 2019) and it has been recently described as an H3K9 mono-methyltransferase that participates in the establishment of heterochromatic loci and in

the maintenance of nuclear lamina (NL) integrity (Pinheiro et al., 2012).

H3K9 methylation has been implicated in the stable silencing and anchoring of heterochromatin at the nuclear periphery, a mechanism that regulates cell fate stabilization and commitment in different metazoan organisms (Gonzalez-Sandoval et al., 2015; Kind et al., 2013; Pinheiro et al., 2012; Poleshko et al., 2017; Towbin et al., 2012). This process has been proposed to depend on cell-type-specific interactions between chromatin and nuclear lamina. However, while chromatin regions that interact with NL (lamin-associated domains or LADs) have been mapped in different cell types (Guelen et al., 2008; Lund et al., 2013; Peric-Hupkes et al., 2010; Poleshko et al., 2017), cell-specific proteins responsible of such tethering mechanism have been not identified yet. Moreover, if such mechanisms mediate FAPs phenotypical plasticity during skeletal muscle regeneration and degeneration has been not addressed.

Here, we found that Prdm16, G9a and GLP are particular enriched in FAPs, as compared to MuSCs. We show that pharmacological inhibition or RNAi-mediated knock-down (KD) of either G9a/GLP and Prdm16 de-repress master myogenic genes in FAPs and induce their myogenic differentiation. Moreover, we provide evidence that Prdm16 controls G9a/GLP-dependent H3K9me2 deposition at muscle-specific loci. We show that H3K9me2 is specifically restricted to a layer of peripheral heterochromatin in FAPs. Of note, Prdm16, G9a and GLP are enriched at the nuclear lamina, where we found confined the genomic loci of master myogenic genes, such as *MyoD*. Finally, using different *in vivo* approaches, comprising FAP-specific ablation of Prdm16, treatment of FAPs-specific reporter mice with a specific G9a/GLP inhibitor and lineage tracing

experiments, we demonstrate that inhibition of Prdm16-G9a/GLP pathway promotes FAPs participation to myogenesis upon induction of skeletal muscle regeneration.

Taken together our data identified a FAPs-specific epigenetic axis critical to maintain the stable silencing of the myogenic program. Notably, we demonstrate that this repression can be reverted by the use of H3K9 KMTs specific inhibitors to reprogram FAPs towards myogenesis, leading to an overall acceleration of the muscle regeneration process.

## Results

### G9a and GLP are enriched in FAPs

To determine the potential role of H3K9 KMTs in FAPs, we first analyzed their expression, and the levels of histone methylation, in FAPs and in MuSCs, derived from both un-perturbed (WT-un-injured) and regenerating (5 days post-cardiotoxin (CTX)-induced injury; 5 d.p.i.) hindlimb skeletal muscles isolated by Fluorescence Activated Cell Sorting (FACS) from 1.5-month-old of PDGFR $\alpha$ -H2B::eGFP mice (Fig. 1A). These mice allow distinct separation of FAPs ( $Lin^{neg}/a7integrin^{neg}/Scal^{pos}/eGFP^{pos}$ ) from MuSCs ( $Lin^{neg}/a7integrin^{pos}/Scal^{neg}/eGFP^{neg}$ ), thanks to the FAPs-specific expression of PDGFR $\alpha$  in adult skeletal muscle (Joe et al., 2010; Tabula Muris et al., 2018; Uezumi et al., 2010; Wosczyzna et al., 2019). Western Blot (WB) analysis for the four major H3K9 KMTs demonstrates that while SUV39h1 levels are identical in FAPs and MuSCs, SETDB1 and G9a/GLP show cell-specific enrichment, with SETDB1 enriched in MuSCs, and G9a/GLP particularly expressed in FAPs (Fig.1 B/C). By contrast, global levels of the different methylated forms of H3K9 (H3K9me1, me2, me3) were substantially similar in FAPs and MuSCs (Fig.1 D), as expected in light of the well-known redundancy of the four H3K9 KMTs in catalyzing the different levels of methylation (Mozzetta et al., 2015). Moreover, G9a immunofluorescence on PDGFR $\alpha$ -H2B::eGFP muscles showed a specific enrichment in GFP $^+$ -FAPs, further supporting a role in FAPs function *in vivo* (Fig. 1E).

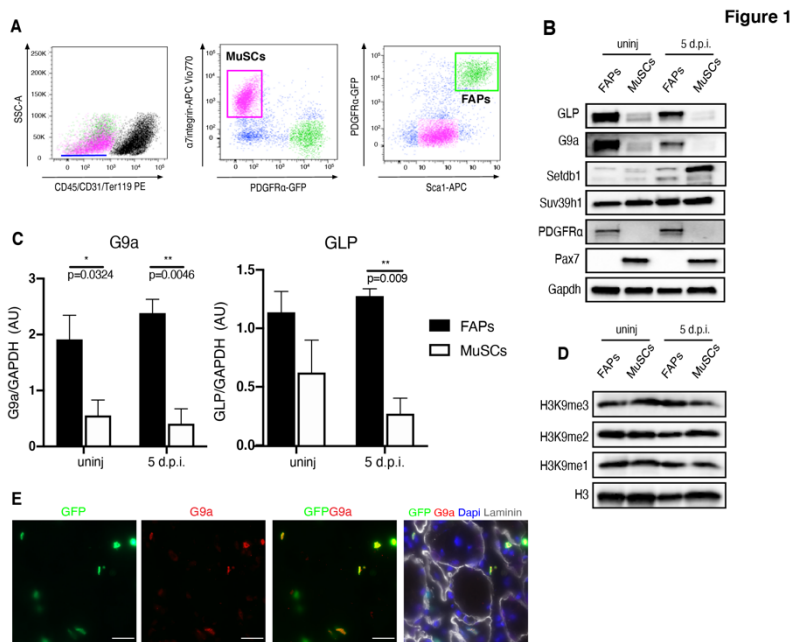


**Figure 1: G9a and GLP are enriched in FAPs**

**A)** FACS plot depicting sorting strategy for FAPs and MuSCs from PDGFRa:H2BeGFP mice. FAPs are isolated as Lineage Negative: Ter119<sup>-</sup>/CD45<sup>-</sup>/CD31<sup>-</sup>, and a7-integrin<sup>-</sup>/Sca1<sup>+</sup>/GFP<sup>+</sup> cells (green box), while MuSCs are isolated as Lineage Negative: Ter119<sup>-</sup>/CD45<sup>-</sup>/CD31<sup>-</sup>, and a7-integrin<sup>+</sup>/Sca1<sup>-</sup>/GFP<sup>-</sup> cells (pink box). **B)** Representative images of Western blot (WB) analysis for the four major H3K9 KMTs (G9a, GLP, SETDB1 and Suv39h1) in FAPs and MuSCs isolated as described in A from un-injured (WT) and injured (5 d.p.i.) PDGFRa:H2BEGFP mice. PDGFRa has been used as a marker of FAPs, while PAX7 as a marker of MuSCs. GAPDH serves as a loading control. **C)** Quantification of densitometry results of WB analyses of G9a and GLP. Protein levels are defined as a ratio on GAPDH, and graphs show the mean of three independent experiments ( $\pm$ sem). **D)** Representative WB analysis H3K9me1, H3K9me2 and H3K9me3 in FAPs and MuSCs isolated as described in C. Total histone H3 has been used as a loading control. **E)** Representative images of immunostaining for G9a (red), GFP (green) and Laminin (grey) on cryo-sections of tibialis anterior of PDGFRa:H2BEGFP mice, 5 d.p.i., in which nuclei were counterstained with DAPI (blue). Scale bar: 100 $\mu$ m. Statistical significance in (C) has been assessed by 2-way Anova. AU (arbitrary units).

## **G9a/GLP silence the myogenic transcriptional program in FAPs**

To gain insights into G9a/GLP function, we performed RNAi-mediated Knock-Down (KD) in FAPs isolated from regenerating muscles (Fig. 2A) (5 d.p.i, a time point at which FAPs are actively proliferating (Lemos et al., 2015)). Since G9a and GLP work predominantly as an heterodimer (Shinkai & Tachibana, 2011), we performed concomitant siRNA-mediated KD of both G9a and GLP, in FAPs cultured *ex-vivo* in growing medium (GM). We then assessed their differentiation capacity in pro-adipogenic differentiation medium (DM) as previously described (Joe et al., 2010; Uezumi et al., 2010) (Fig. 2A). Western blot analysis confirmed G9a and GLP down-regulation (Fig. 2B). Strikingly, while control (siScr) FAPs massively differentiated into perilipin-positive adipocytes upon induction of differentiation (Fig. 2C and Supplementary 1A), as previously reported (Joe et al., 2010; Uezumi et al., 2010), G9a/GLP KD (siG9aGLP) induced the formation of Myosin Heavy Chain (MyHC) positive myotubes (Fig. 2C) and reduced the formation of Perilipin<sup>+</sup> adipocytes (Fig. 2C and Supplementary 1A). This result was further confirmed by WB (Fig. 2D), through which we could appreciate expression of MyHC in siG9a/GLP FAPs, and reduced levels of  $\alpha$ -Smooth Muscle Actin ( $\alpha$ SMA), a fibrotic marker, and Perilipin (Fig. 2D). Consistently, qRT-PCR analysis demonstrated that G9a/GLP KD leads to reduced expression of adipogenic genes (*Plin1*, *Adipoq*, *Ap2*) (Fig. 2E) and enhanced transcription of key genes involved in muscle differentiation (*MyoD*, *Myf5*, *Myh3*, *Myh8*, *Des*) (Fig. 2F). These data led us to conclude that G9a/GLP silence FAPs myogenic developmental capacity. To further support this, we assessed genomic occupancy of the G9a/GLP-deposited histone mark and we found regulatory genomic loci of key myogenic genes (*MyoD*

transcriptional start site, *TSS*; *MyoD* core enhancer, *CE*; *Des*) considerably enriched in H3K9me2 in FAPs, as compared to MuSCs (Fig. 2G), in line with their repressed status (Joe et al., 2010). By contrast H3K9me2 levels on *AP2* locus, encoding for a marker of adipogenic differentiation (Ohno et al., 2013), were higher in MuSCs than FAPs (Fig. 2G). Taken together, these data led us to conclude that G9a/GLP-mediated H3K9 methylation are responsible to maintain the stable repression of a myogenic transcriptional program in FAPs.

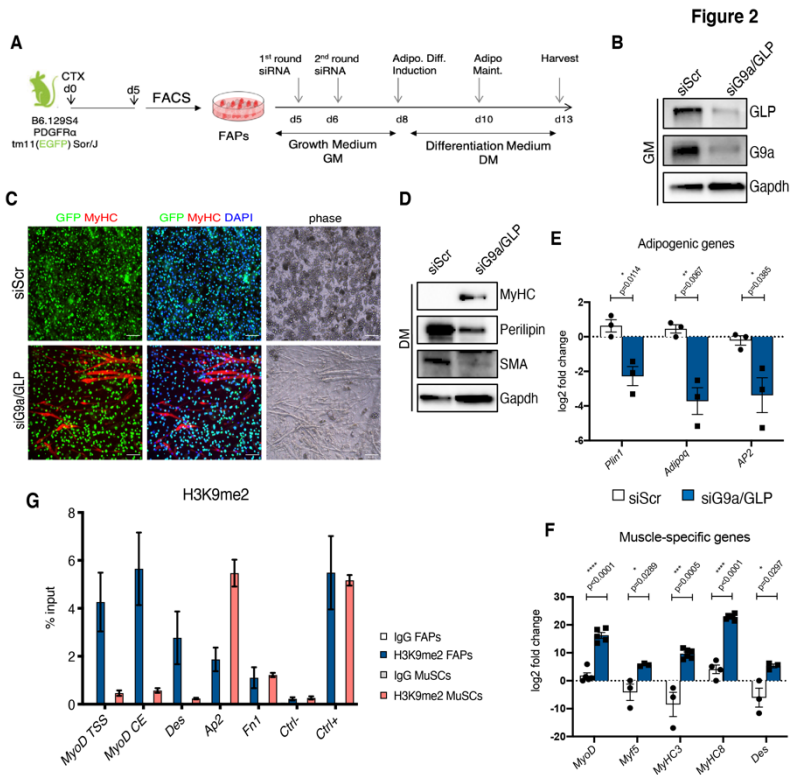


**Figure 2: G9a/GLP knock-down induces the acquisition of a myogenic phenotype and decreases FAPs' fibro-adipogenic differentiation**

**A)** Schematic representation of concomitant siRNA-mediated KD of both G9a and GLP in FAPs, FACS-isolated from PDGFR $\alpha$ -H2BeGFP mice 5 d.p.i, are cultured ex-vivo in growth medium (GM) and then induced to differentiate in adipogenic differentiation medium (DM). **B)** Western blot analysis of G9a and GLP in FAPs upon G9a/GLP KD (siG9a/GLP) as compared to control FAPs transfected instead with scrambles siRNA (siScr); GAPDH levels are shown as loading control. **C)** Representative images of immunofluorescence for Myosin Heavy Chain (MyHC; red), and GFP autofluorescence (green,) of PDGFR $\alpha$ -GFP<sup>+</sup> FAPs cultured as described in (A) and induced to differentiate. Nuclei are counterstained with DAPI (blue) and phase contrast images are shown on the right. Scale bar: 100 $\mu$ m. **D)** WB analysis for the indicated proteins (MyHC, as a marker of myogenic differentiation;  $\alpha$ -Smooth Muscle Actin ( $\alpha$ SMA), as a marker of fibrotic cells; Perilipin, as a marker of mature adipocytes) in control FAPs (scr) and FAPs upon G9a/GLP KD (siG9a/GLP), induced to differentiate. GAPDH has been used as loading control. **E)F)** qRT-PCR analysis of adipogenic (E) (*Plin1*, *Adipoq*, *AP2*) and myogenic (F) (*Myf5*, *MyoD*, *Myhc3*, *Myhc8*, *Des*) transcripts of FAPs grown in DM and cultured as described in (A). The histograms show the mean log<sub>2</sub> fold change value derived from  $n \geq 3$  independent experiments ( $\pm$ s.e.m.). Statistical significance has been assessed by t-test and the p values are shown on the graphs (\*  $p < 0.05$ ; \*\*  $p < 0.01$ ; \*\*\*  $p < 0.001$ ; \*\*\*\*  $p < 0.0001$ ). **G)** ChIP-qPCR analyses of H2K9me2 enrichment on the indicated regions in FAPs (blue bars) and MuSCs (red bars) cultured in GM. Enrichment is expressed as a percentage of input (% input) and the histograms show the mean value derived from  $n=2$  independent ChIP experiments on different chromatin preparations. IgG were used as negative control of enrichment. *MyoD* CE (core enhancer), *MyoD* TSS (transcription start site) and *Des* promoter were used as representative muscle-specific loci. *Ap2* as an adipogenic marker expressed by FAPs and *Fn1* (fibronectin) promoter as a gene expressed in FAPs and MuSCs. *Ctrl+*, is a region constitutively enriched for H3K9me2, and *Ctrl-*, (*Ube2b* promoter,) a region constitutively devoid of H3K9me2, served us as IP controls.

## **Prdm16 is a FAP-specific, nuclear lamina-enriched factor, that mediates H3K9me2 deposition at muscle-specific loci**

GLP has been identified as the H3K9 methyltransferase activity of the Prdm16 transcriptional complex (Ohno et al., 2013). Intriguingly, Prdm16 has been also recently described as an H3K9 mono- methyltransferase that participates in the establishment of silent heterochromatic loci (Pinheiro et al., 2012). In particular, it has been shown that Prdm16 works as a cytoplasmic enzyme to direct H3K9 mono-methylation (H3K9me1) on free histone H3, and this is essential to maintain heterochromatin clustering and the structure of the nuclear lamina (Pinheiro et al., 2012). These evidences, together with the well-known role of Prdm16 as a myo-adipogenic switch of common Myf5<sup>+</sup> precursors (Ohno et al., 2013; Seale et al., 2008), stimulated our interest in investigating a possible interplay between Prdm16 and G9a/GLP in FAPs. To this end we first assessed its expression and we found that FAPs specifically express Prdm16, as compared to MuSCs (Fig. 3A). Proximity Ligation Assay (PLA) confirmed GLP and Prdm16 interaction in FAPs, which revealed a peculiar peri-nuclear localization (Fig. 3B). As a positive control, we assessed G9a/GLP interaction, confirming that G9a/GLP interact instead predominantly in the nuclear interior (Supplementary 2A), as already reported in other cell types (Shinkai & Tachibana., 2011). Consistently, immunofluorescence (IF) demonstrates Prdm16 co-localization with the nuclear lamina (NL), marked by LaminB and Lamin A/C, both at the endogenous level (Fig. 3C) and after over-expression of a FLAG-tagged form of Prdm16 in FAPs (Fig. 3D). This localization was confirmed in Prdm16-expressing cell types, such as the brown-preadipocytes WT-1 (Tseng et al., 2004) (Supplementary 2B) and after over-expression in 293T (Supplementary 2C), suggesting a conserved perinuclear function of Prdm16. This evidence was further

supported by biochemical fractionation experiments, which confirmed that G9a, GLP and Prdm16 preferentially segregate in the NL fraction, enriched in LaminB and Lamin A/C (Fig. 3E). Nuclear lamina is a well-known nuclear compartment rich in heterochromatin, where genes that have to be maintained stably repressed are spatially confined (Kind J et al Cell., 2013). Prdm16 co-localization with LaminB and the evidence that Prdm16 is able to recruit G9a and GLP to the chromatin of genes to mediate their silencing (Ohno et al., 2013), led us to speculate that Prdm16 might cooperate with G9a/GLP to maintain the repression of myogenic-specific genes in FAPs by confining them to the nuclear periphery. To provide evidence of Prdm16 requirement in mediating G9a/GLP-dependent silencing of muscle-specific genes, we first demonstrated that Prdm16 KD (siPrdm16) recapitulated the phenotype observed decreasing G9a/GLP expression. In fact, siPrdm16 FAPs displayed MyHC expression and reduction of aSMA and Perilipin, as compared to control (siScr) FAPs (Fig. 3F). Consistently, while siScr FAPs massively differentiated into perilipin-positive adipocytes upon induction of differentiation (Fig. 3G), siPrdm16 induced the formation of Myosin Heavy Chain (MyHC) positive myotubes and reduced FAPs differentiation into Perilipin<sup>+</sup> adipocytes (Fig. 3G and Supplementary 2D). Accordingly, qRT-PCR analysis revealed reduction of adipogenic-specific transcripts (*PPAR $\gamma$* , *Fabp4*, *Cebpa*) and increased expression of myogenic-specific genes (*Myf5*, *MyoD*, *Des*) (Supplementary 2E), further supporting a role of Prdm16 in maintaining the repression of the myogenic program in FAPs. To verify if Prdm16 mediates G9a/GLP-dependent deposition of H3K9me2 at myogenic loci in FAPs, we performed Chromatin Immunoprecipitation (ChIP) of H3K9me2 in FAPs upon siRNA-mediated KD of Prdm16 (siPrdm16). This analysis demonstrated that the regulatory regions of muscle-specific genes (*MyoD*, *Myf5*

and *Des*) are particularly enriched in H3K9me2 in control FAPs (Scramble, Scr), as compared to MuSCs (Fig. 3H) and as also shown in Fig. 2G, coherently with their transcriptional repressed status. Notably, although global levels of H3K9me2 were unaffected in siPrdm16 FAPs (Supplementary 2F), Prdm16 KD reduced H3K9me2 levels at these loci (Fig. 3H), consistent with their induced expression (Supplementary 2E). Taken together, these results led us to conclude that Prdm16 mediates G9a/GLP-dependent deposition of H3K9me2 at muscle-loci in FAPs, thereby maintaining their epigenetic silencing.

**Figure 3**

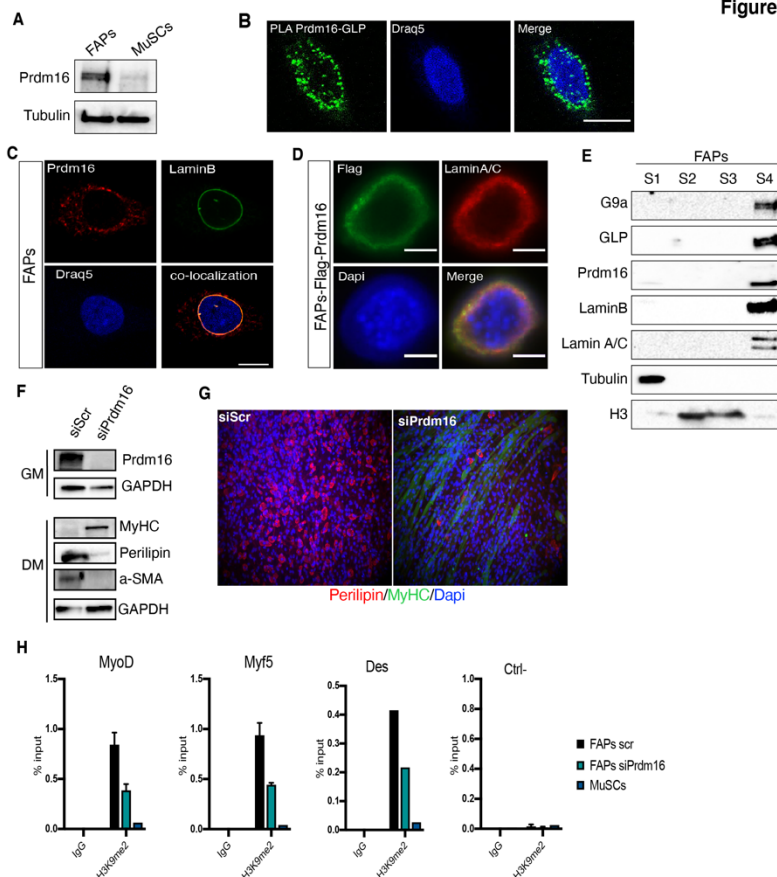


**Figure 3: Prdm16 mediates G9a/GLP-dependent H3K9me2 deposition at muscle specific loci**

**A)** Representative images of WB analysis of Prdm16 in FAPs and MuSCs isolated from 5 d.p.i. skeletal muscles. Tubulin is shown as a loading control. **B)** Representative confocal microscopy images of Proximity Ligation Assay (PLA) assay between Prdm16 and GLP. Fluorescent dots (green) represent the proximity sites of GLP and PRDM16. Nuclei were counterstained with Draq5 (blue). Scale bar: 10µm. **C)** Immunofluorescence for endogenous Prdm16 (red) and Lamin B1 (green) in FAPs cultured ex-vivo. Nuclei were counterstained with Draq5 (blue). Representative images are shown. Co-localization has been evaluated with confocal microscopy. Scale bar: 10 µm. **D)** Representative images of immunofluorescence for FLAG (green) and Lamin A/C (red) in FAPs overexpressing Flag-Prdm16.

Nuclei are counterstained with DAPI. Scale bar: 5 $\mu$ m. **E)** Representative images of WB analyses of chromatin fractionation experiments performed on FAPs from WT C57BL/10 mice. Equal amounts of each fraction were immunoblotted and hybridized with indicated antibodies. Positive controls: Tubulin (S1), Histone H3 (S2, S3), and Lamin A/C, LaminB (S4). **F)** Representative images of WB analysis for the indicated proteins in FAPs subjected to siPrdm16 transfection, as compared to siScr-transfected FAPs. Prdm16 KD has been assessed before induction of differentiation (in GM) and MyHC, Perilipin and aSMA levels were instead analysed upon differentiation (DM). GAPDH is shown as a loading control. **G)** Representative images of immunofluorescence for MyHC (green) and Perilipin (red) in differentiating FAPs cultured in adipogenic DM after Prdm16 KD (siPrdm16), as compared to control FAPs (siScr). Nuclei were counterstained with DAPI (blue). **H)** ChIP-qPCR analysis of H3K9me2 in FAPs cultured ex-vivo in growth medium upon to siRNA-mediated KD of Prdm16 (siPrdm16), as compared to scramble-transfected FAPs (siScr) and to MuSCs. Enrichment is expressed as a percentage of input (% input) and the histograms show the mean value derived from n=3 (+/- sem) independent experiments on different chromatin preparations. IgG were used as negative control of enrichment. Ube2b promoter, a region constitutively devoid of H3K9me2, served us as controls.

## ***In vivo* FAPs-specific ablation of Prdm16**

The data presented above revealed a central role played by Prdm16 in preserving FAPs identity. To gain further insights into the FAPs-specific function of Prdm16 *in vivo*, we decided to specifically and conditionally ablate it in FAPs. To this end, we crossed Prdm16<sup>Flox/Flox</sup> with PDGFRa<sup>Cre-ERT/+</sup> mice (PDGFRatm13Sor/J, already successfully used to perform conditional FAP-specific KO by different groups (Heredia et al., 2013; Kopinke et al., 2017; Lemos et al., 2015)). To conditionally induce Cre Recombinase, we intra-peritoneally injected tamoxifen (TMX) for 5 consecutive days to young adult Prdm16<sup>Flox/Flox</sup>:PDGFRa<sup>Cre-ERT/+</sup> double transgenic mice (hereafter referred to as FAPs<sup>Prdm16cKO</sup>) Prdm16<sup>Flox/Flox</sup>:PDGFRa<sup>+/+</sup> mice, without the Cre, were used as control (referred to as FAPs<sup>Ctrl</sup>) (Fig. 4A). After TMX injection, 5 days before the isolation of FAPs we induced skeletal muscle regeneration by intra-muscular CTX injection (Fig. 4A). WB analysis confirmed down-regulation of Prdm16 protein in FAPs isolated from FAPs<sup>Prdm16cKO</sup> mice (Fig. 4B). Strikingly, reduction of Prdm16 induced FAPs to express MyHC and to decrease Perilipin levels (Fig. 4B). In agreement with this result, when cultured under differentiating conditions, FAPs from FAPs<sup>Prdm16cKO</sup> mice formed myotubes, as compared to FAPs isolated from control mice (FAPs<sup>Ctrl</sup>) that differentiated instead, as expected, into adipocytes (Fig. 4C). Accordingly, qRT-PCR analysis confirmed induction of myogenic genes (*MyoD*, *Myf5*, *Des*) (Fig. 4D). Importantly, clonal analysis confirmed that while FAPs<sup>Ctrl</sup> were able to give rise only to fibro-adipogenic clones, FAPs<sup>Prdm16cKO</sup> formed instead also myogenic clones, while reducing their fibro- and adipogenic potentials (Fig. 4E; Supplementary 3). Of note, by CHIP we

observed decreased H3K9me2 levels at regulatory regions of the master myogenic gene *MyoD* upon Prdm16 *in vivo* loss-of-function; and a reduction of the LaminB occupancy in FAPs<sup>Prdm16cKO</sup>, suggesting that MyoD transcriptional induction (Fig. 4D) is a consequence of H3K9me2 loss caused by Prdm16 downregulation, which also likely impairs contacts with NL (Fig. 4F).

Finally, to assess the impact of the acquisition of a myogenic fate by FAPs upon reduction of Prdm16 *in vivo*, we analyzed the overall muscle regeneration process by evaluating myofibers' cross sectional area (CSA) and the percentage of embryonic MyHC<sup>+</sup> fibers. Immunostaining of muscles 5 d.p.i. revealed that FAPs<sup>Prdm16cKO</sup> myofibers had an increased CSA (Fig. 4G-I) and a decreased percentage of regenerating fibers, as compared to FAPs<sup>Ctrl</sup> muscles (Fig. 4G and L). This was also accompanied by reduced fat infiltration, as demonstrated by the reduction in Perilipin<sup>+</sup> infiltrating cells in FAPs<sup>Prdm16cKO</sup> muscles, as opposed to FAPs<sup>Ctrl</sup> muscles (Fig. 4M and N).

Taken together, these results demonstrate that FAPs-specific Prdm16 ablation induces these cells to acquire a myogenic phenotype *in vivo*, thus promoting an overall acceleration of the muscle regenerative process.

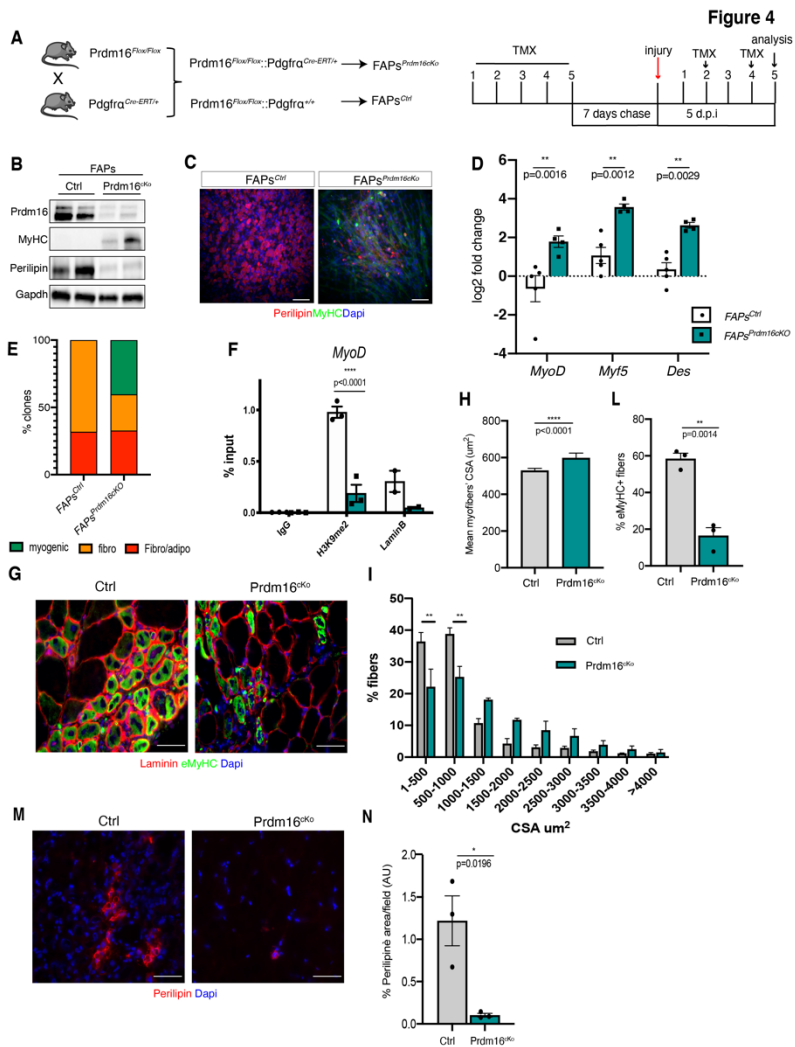


**Figure 4: *Prdm16* ablation in FAPs induces the acquisition of a myogenic phenotype *in vivo***

**A)** Schematic representation of the experimental design showing the breeding scheme used to develop mice to conditionally ablate *Prdm16* in FAPs (left) and the schedule of tamoxifen (TMX) treatment (right). All mice were treated for 5 consecutive days with TMX, by

intraperitoneal injection. After 7 days, muscle regeneration was induced with CTX, via intramuscular injection. Muscles and FAPs were then isolated 5 d.p.i. **B)** Representative images of Prdm16, MyHC and Perilipin WB analysis in FAPs derived from both FAPs<sup>Ctrl</sup> and in FAPs<sup>Prdm16cKO</sup> mice, cultured ex-vivo. GAPDH has been used as a loading control. **C)** Representative images of immunofluorescence for MyHC (green) and Perilipin (red) in FAPs derived from both FAPs<sup>Ctrl</sup> and in FAPs<sup>Prdm16cKO</sup> mice, cultured ex-vivo and induced to differentiate. Nuclei were counterstained with DAPI (blue). Scale bar: 100µm. **D)** qRT-PCR analysis of myogenic (Myf5, MyoD, Des) markers in FAPs derived from both FAPs<sup>Ctrl</sup> and in FAPs<sup>Prdm16cKO</sup> mice cultured ex-vivo in growing medium. The histogram shows the mean log<sub>2</sub> fold change value, for each gene, derived from FAPs isolated from n≥3 mice (±s.e.m.) (\*\* p<0.01; assessed by t-test). **E)** The histogram shows quantification of the percentage of myogenic, adipogenic and fibro-adipogenic clones found after growing FAPs<sup>Ctrl</sup> and FAPs<sup>Prdm16cKO</sup> clonally 23 days in growing conditions. **F)** ChIP-qPCR analysis to evaluate H3K9me2 and Lamin B1 occupancy at MyoD TSS both in FAPs<sup>Ctrl</sup> (white bars) and in FAPs<sup>Prdm16cKO</sup> (green bars) cells. **G)** Representative images of immunostaining for Laminin (red), the embryonic MyHC isoform (eMyHC, green) on cryosections of Ctrl and in Prdm16cKO mice 5 d.p.i. Nuclei were counterstained with DAPI (blue). Scale bar: 50µm. **H)** The histogram shows the mean cross-sectional area (CSA) of myofibers of FAPs<sup>Ctrl</sup> and FAPs<sup>Prdm16cKO</sup> muscles 5 d.p.i. Data derive from n=3 mice and are shown as mean +/- sem (\*\*\*\* p<0.0001; assessed by t-test). **I)** The graph shows the distribution of Myofibers CSA of muscles shown in G, as the percentage of myofibers within the indicated CSA range. Statistical significance has been assessed by 2-way Anova and Sidak's multiple comparison test (\*\*\* p< 0.001). **L)** Histogram shows the percentage of eMyHC<sup>+</sup> fibers in Ctrl and Prdm16cKO muscles 5 d.p.i. Data derive from n=3 mice and are shown as mean +/- sem (\*\* p<0.01; assessed by t-test). **M)** Representative images of immunostaining for Perilipin (red) on cryosections of Ctrl and in Prdm16cKO mice 5 d.p.i. Nuclei were counterstained with DAPI (blue). Scale bar: 50µm. **N)** The histogram shows the percentage of Perilipin positive infiltrate in Ctrl and in Prdm16cKO muscles 5 d.p.i. Data derive from n=3 mice and are shown as mean +/- sem (\*p<0.01; assessed by t-test).

## **Prdm16 preserves nuclear integrity and mediates H3K9me2-dependent tethering of muscle loci at the nuclear lamina**

In light of the peripheral localization of Prdm16/GLP interacting dots (Fig. 3B) and its association with NL (Fig. 3C/D), we reasoned that Prdm16-G9a/GLP-mediated H3K9me2 might serve to silence myogenic genes confining them at the nuclear periphery. In support of this hypothesis, immunofluorescence of the different H3K9 methylation marks in FAPs showed that while both H3K9me1 and H3K9me3 formed foci mostly interspersed in the nuclear interior, H3K9me2 forms instead a peripheral layer beneath the nuclear lamina, as also previously reported in other cell types (Fig. 5A) (Poleshko et al 2017).

To test the functional relevance of H3K9me2 in the NL-tethering of muscle specific loci, we treated FAPs with a G9a/GLP specific inhibitor, A-366 (Pappano et al., 2015), which efficiently reduced H3K9me2 global levels (Fig. 5B), and we then assessed subnuclear localization of the genomic loci of the master myogenic gene *MyoD*, by immuno DNA-Fluorescence In Situ Hybridization (FISH) (Fig. 5C and D). Notably, while in untreated FAPs *MyoD* genomic loci were found in close proximity with nuclear lamina (Fig. 5C and D), A-366 treatment induced a significant re-localization of *MyoD* loci towards the nuclear interior (Fig. 5C and D). Strikingly, this was accompanied by *MyoD* transcriptional induction (Fig. 5E) and the consequent capacity of FAPs to spontaneously enter the muscle terminal differentiation program, as assessed by the formation of MyHC<sup>+</sup> myotubes (Fig. 5F).

Then, to verify the role of Prdm16 in mediating *MyoD* genomic subnuclear localization we performed immuno-DNA FISH in FAPs<sup>Ctrl</sup> and in FAPs<sup>Prdm16cKO</sup>. Surprisingly, we observed a significant percentage of FAPs<sup>Prdm16cKO</sup> to be polyploid for *MyoD* loci (mostly tetraploid; Fig. 5G and H). Moreover, LaminB

immunofluorescence revealed NL defects, as nuclei of FAPs<sup>Prdm61cKO</sup> displayed nuclear invagination (Fig. I), a typical defect observed in nuclei defective for NL-associated proteins (Kubben and Misteli., 2017). This observation agrees with previous results showing disruption of the NL in MEFs depleted of both Prdm16 and its homologue Prdm3 (Pinheiro et al., 2012), and further support a role of Prdm16 as a NL-associated factor important for the heterochromatin tethering at the nuclear periphery. To provide further support of this, we analyzed H3K9me2 and H3K9me3 by immunostaining in FAPs<sup>Prdm16cKO</sup> and FAPs<sup>ctr</sup>. Strikingly, the peripheral localization of H3K9me2 observed in FAPs<sup>ctr</sup> was lost in FAPs<sup>Prdm16cKO</sup>, where it became more dispersed towards the nuclear interior (Fig. 5L). By contrast, H3K9me3 did not show evident signs of mislocalization, as H3K9me3<sup>+</sup> heterochromatic foci were present in both FAPs<sup>Prdm16cKO</sup> and FAPs<sup>ctr</sup> (Fig. 5M).

Figure 5

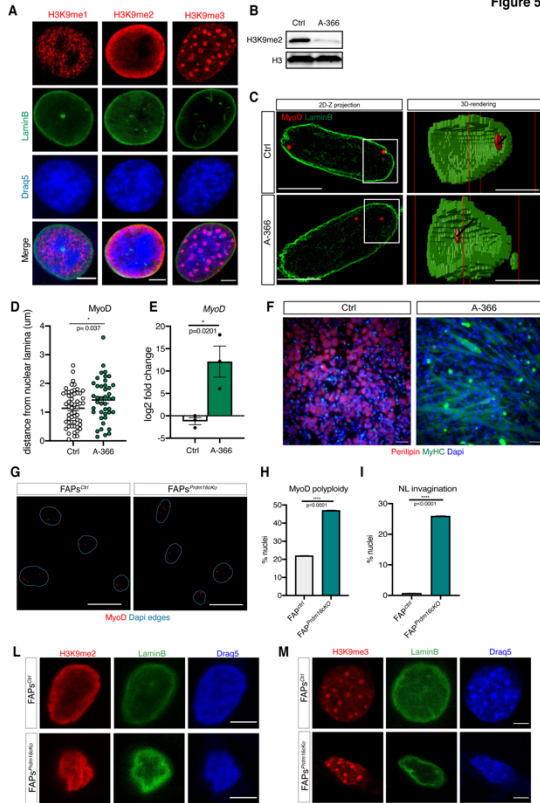


**Figure 5: H3K9me2 mediates tethering of MyoD at the nuclear periphery and Prdm16 maintains nuclear lamina integrity**

**A)** Representative images of immunofluorescence for H3K9me1, H3K9me2, H3K9me3 (red) and LaminB (green) in FAPs cultured ex-vivo in GM. Nuclei are counterstained with Draq5 (blue). Scale bar: 5µm. **B)** Evaluation of H3K9me2 global levels by WB in FAPs cultured in the presence (A-366) or absence (ctrl) of the G9a/GLP specific inhibitor A-366 (1nM) for 48h in GM. **C)** Representative Immuno-DNA FISH of myoD locus (red spots) co-stained for Lamin B (green) in WT FAPs cultured as described in B. Left panels show myoD locus in relation to nuclear lamina in a 2D maximum intensity projection of Z-stacks (scale bar: 10µm). The magnifications on the right show a 3D-rendering of the specific region highlighted with a white square (scale bar: 4µm). The black lines represent the minimal 3D-distance between the spots of MyoD and the lamina. **D)** The graph shows the quantification of 3D-distance between MyoD locus and nuclear lamina performed on an individual locus basis. Statistical significance has been assessed by t-test. \*  $p < 0.05$ . **E)** MyoD mRNA levels evaluated by qRT-PCR in FAPs cultured as in B and C. The graph shows the mean  $\log_2$  fold

change (+/- sem) of  $n=3$ . Statistical significance has been assessed by t-test: \*  $p<0.05$ . **F**) Representative images of immunofluorescence for MyHC (green) and Perilipin (red) in FAPs treated for 48h with A-366 (as in B) compared to untreated (ctrl) cells. Nuclei were counterstained with DAPI (blue). Scale bar:  $100\mu\text{m}$ . **G**) Representative images of MyoD DNA FISH (red spots) in FAPs derived from  $FAPs^{Ctrl}$  and in  $FAPs^{Prdm16cKO}$  mice. In blue nuclear edges are depicted based on Dapi staining. Scale bar:  $25\mu\text{m}$ . **H**) Histogram shows the percentage of nuclei showing  $n>2$  MyoD loci of FAPs described in G. **I**) Histogram shows the percentage of nuclei showing nuclear lamina invagination inside the nuclear interior, assessed by LaminB immunofluorescence in FAPs derived from  $FAPs^{Ctrl}$  and in  $FAPs^{Prdm16cKO}$  mice. **L**) **M**) Representative images of immunofluorescence for H3K9me2 (L) and H3K9me3 (M) in  $FAPs^{Ctrl}$  and  $FAPs^{Prdm16cKO}$ . LaminB is show in and nuclei are counterstained with Draq5 (blue). Scale bar:  $5\mu\text{m}$ .

## **FAPs participate to skeletal myogenesis *in vivo* upon inhibition of H3K9 di-methylation**

The data presented above clearly point towards a Prdm16-G9a/GLP-dependent mechanism of H3K9 methylation responsible to silence the myogenic transcriptional programs in FAPs. These results led us to hypothesize that this pathway might be targeted pharmacologically to de-repress myogenic genes in FAPs to induced them to participate to myogenesis *in vivo*.

To test this, we induced muscle regeneration by intramuscular injection of CTX on PDGFR $\alpha$ :H2B-eGFP mice and we then treated a group of mice with daily intra-peritoneal injection of A-366, for 5 days, while another group was treated with vehicle as control (Fig. 6A). Immunofluorescence analysis for GFP and Laminin on muscle cryosection of CTRL- and A-366-treated mice revealed that G9a/GLP inhibition induced FAPs to participate in skeletal myogenesis, as demonstrated by the presence of GFP<sup>+</sup> FAPs within regenerating myofibers (Fig. 6B-D). Accordingly, FAPs isolated from A-366-treated mice displayed a spontaneous propensity to form myotubes *ex-vivo*, as compared to FAPs isolated from CTRL-treated muscles, which instead differentiate into adipocytes (Fig. 6E).

To provide further support of the capacity of FAPs to participate directly to myogenesis *in vivo* upon inhibition of G9a/GLP, we performed a FAPs-lineage tracing experiment in collaboration with Prof. Sigmar Stricker's lab, who developed a murine model to specifically trace activated FAPs *in vivo*. Particularly, Stricker's group demonstrated that transcription factor Odd skipped-related 1 (Osr1) is specifically expressed by a sub-population of activated FAPs upon acute muscle injury (Vallecillo-Garcia et al. 2017, Stumm et al., 2018). To trace Osr1<sup>+</sup>-FAPs *in vivo* they generated an inducible reporter mouse model,

Osr1GCE/+;R26RmTmG/+, derived breeding Osr1eGFP-IRES-CreERT2 (Osr1GCE) X Rosa26-mTmG (R26RmTmG) mice. In this inducible murine model, TMX administration results in Osr1-expressing cells (FAPs), and their progeny, to be permanently labelled by membrane GFP (mGFP). To trace FAPs fate upon inhibition of G9a/GLP, we first administered TMX and we concomitantly induced intramuscular injury with CTX to tibialis anterior (TA). After a second day of TMX injection, and two days of recovery, we then treated a group of mice with vehicle (as control, Ctrl) and another group of mice with A-366 (2mg/kg), for 5 consecutive days. At day 10 post-injury (10 d.p.i.) TA were collected and analyzed (Fig. 6F). In agreement with our previous results, immunofluorescence analysis for Laminin and mGFP, revealed the presence of a significant percentage of myofibers (Laminin<sup>+</sup>) co-stained with mGFP in muscles derived from A-366-treated mice (Fig. 6 G and H), as compared to Ctrl-treated animals. This results further corroborate our initial hypothesis and unequivocally demonstrates the capacity of FAPs to participate to myogenesis *in vivo* upon inhibition of G9a/GLP.

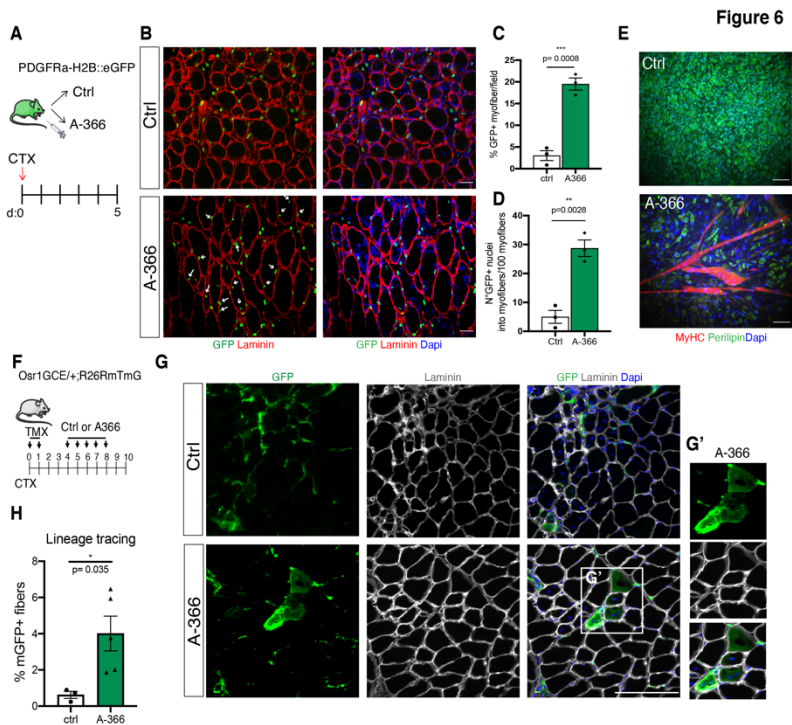


**Figure 6: FAPs participate to skeletal myogenesis in vivo upon G9a/GLP inhibition**

**A**) Schematic representation of the experimental design. Skeletal muscle regeneration is induced in PDGFRa:H2BGFP mice by intra-muscular injection of CTX at day0. A group of mice was treated daily with A-366 (2mg/kg, via intraperitoneal injections), while another group was treated with vehicle as control ( $n=3$  mice/group). Muscles and FAPs were isolated 5 d.p.i. **B**) Representative images of immunostaining for GFP (green) and Laminin (red) on TA cryo-sections of mice treated as in A. Arrowheads highlight GFP<sup>+</sup> nuclei inside Laminin<sup>+</sup> myofibers. Scale bar: 100 $\mu$ m. **C**) **D**) Histograms show the quantification of the percentage of myofibers positive for GFP (C) and the number of GFP<sup>+</sup> nuclei inside the myofibers (D) in muscles shown in B. **E**) Representative IF images of FAPs isolated from Ctrl- and A-366-treated PDGFRa:H2BGFP mice cultured ex-vivo without treatment and induced to differentiate. Nuclei are counterstained with DAPI (blue). Scale bar: 100 $\mu$ m. **F**) Schematic representation of the experimental design. Skeletal muscle regeneration is induced in the tibialis anterior (TA) of Osr1GCE<sup>+/+</sup>;R26RmTmG<sup>+/+</sup> mice by intra-muscular injection of CTX at day 0, in concomitance to Tamoxifen (TMX) administration. Upon 2 consecutive days of TMX and 2 days of wash-out, a group of mice was then treated with 5 daily IP injections of A-366 (2 mg/kg), while another group with vehicle as control (Ctrl) ( $n\geq 3$  mice/group). Muscles were collected 10 d.p.i. **G**) Representative IF images of TA transverse sections from

*Ctr-* and *A-366-treated Osr1GCE/+;R26RmTmG/+* mice stained for mGFP (green) and Laminin (grey). Nuclei were counterstained with DAPI (blue). Scale bar: 100 $\mu$ m. **G'** shows magnification of the white box highlighted in **G**. **H**) Histogram shows the quantification of the percentage of mGFP positive myofibers on sections shown in **G**. Data are presented as the mean ( $\pm$  sem) of the percentage derived from  $n \geq 3$  mice (\* $p < 0.05$ , t-test).

To provide therapeutic relevance of this approach, we then assessed the impact of G9a/GLP inhibition on the overall muscle regeneration process. Strikingly, assessment of myofibers' caliber and maturation of the regeneration, by mean of immunofluorescence for Laminin and the embryonic form of myosin heavy chain (eMyhC) (Fig. 7A), revealed that A-366 treatment induced an increase in myofibers' CSA (Fig. 7B) and a decreased in the percentage of immature (eMyH<sup>+</sup>) myofibers (Fig. 7C).

Taken together our data clearly point towards G9a/GLP-mediated H3K9 methylation as a major epigenetic silencing pathway involved in the control of alternative lineages in FAPs during skeletal muscle regeneration. More importantly, these results identify G9a/GLP as possible pharmacological targets to be exploited to accelerate the muscle regeneration process *in vivo*.

Figure 7

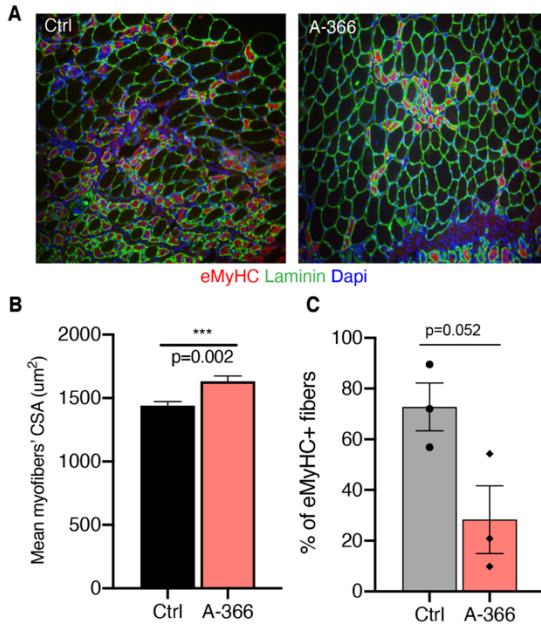


Figure 7: *G9a/GLP inhibition accelerates muscle regeneration in vivo*

*A*) Representative images of immunostaining for Laminin (green), the embryonic MyHC isoform (eMyHC, red) and Dapi (blue) on cryosections of TA derived from wt Ctrl- and A-366 treated mice 5 d.p.i. *B*) The histogram shows the mean cross-sectional area (CSA) of myofibers. Data derive from  $n=3$  mice and are shown as mean  $\pm$  sem (\*\*\*)  $p<0.002$ ; assessed by *t*-test). *C*) Histogram shows the percentage of eMyHC<sup>+</sup> fibers in Ctrl- and A-366 muscles 5 d.p.i. Data derive from  $n=3$  mice and are shown as mean  $\pm$  sem (*p* value assessed by *t*-test).

## **H3K9 KMTs accumulate in FAPs from degenerating dystrophic muscles**

Duchenne muscular dystrophy (DMD) is a severe human myopathy in which the mutation in the *dmd* gene encoding for Dystrophin cause a progressive myofiber degeneration, fibrosis and replacement of muscle tissue with adipocytes (Hoffman et al., 1987). In light of the fact, that H3K9 methylation controls FAPs identity and together with the important role of FAPs during skeletal muscle regeneration, we wanted to assess H3K9 KMTs enrichment in FAPs from different stages of disease progression. Since, as stated above, FAPs from old degenerating dystrophic mice are resistant to HDACi-induced chromatin plasticity (Mozzetta et al., 2013; Saccone et al., 2014), we speculate that H3K9 KMTs might represent an epigenetic barrier that constraints FAPs developmental capacities. To provide preliminary evidence in this direction, we isolated from *Dmd*<sup>mdx</sup> mice (MDX), the spontaneous mutant mice which do not express dystrophin, which represents the murine model of DMD. To model early phases of DMD, when muscle regeneration is still ongoing, and late stages of the disease, when dystrophic muscles are already degenerated, we isolated FAPs from young (1,5 months) and old (>1 year) MDX mice, respectively (as in Mozzetta et al., 2013). Interestingly, WB analysis revealed that G9a, GLP, and Prdm16 are markedly enriched in FAPs from old degenerating dystrophic muscles, as compared to young muscles (Fig. 8A). Consistently, chromatin fractionation experiments show an accumulation of G9a, GLP and Prdm16 at the nuclear lamina compartment, rich in LaminB and Lamin A/C, in FAPs from old MDX mice (Fig. 8B). These results suggest that in degenerating dystrophic muscle the aberrant accumulation of Prdm16/G9a/GLP might be responsible to lock FAPs chromatin and restrict their plasticity. The functional

relevance of this observation will be matter of investigation in our future experiments.

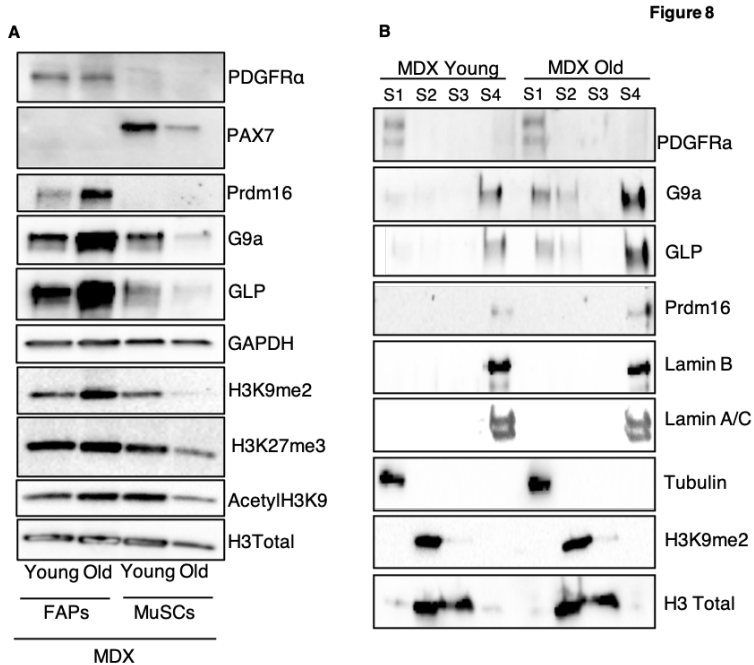


**Figure 8: H3K9 KMTs are enriched in FAPs from old dystrophic muscles respect to MDX Young mice and preferentially associated with nuclear lamina**

**A)** Western blot analysis of FAPs and MuSCs isolated from young (1,5 months) and old (>1 year) MDX mice reveals that G9a, GLP and PRDM16 are enriched in FAPs from dystrophic muscles respect to MuSCs, particularly in FAPs from Old MDX mice. Western blot analysis shows also that, FAPs isolated from Old MDX mice, possess a high level of H3K9me2 respect Young MDX mice and also respect to the SCs. For this analysis we process a group of three Young MDX mice and a group of three Old MDX mice. **B)** Chromatin fractionation (S1, S2, S3, S4) of FAPs from Young an Old MDX mice (n=3). Equal amounts of each fraction were immunoblotted and hybridized with indicated antibodies. Positive controls: Tubulin (S1), Histone H3 (S2, S3), and Lamin A/C, Lamin B (S4). This analysis show that G9a, GLP and PRDM16 associate with the nuclear lamina compartment rich in LaminB and Lamin A/C and in particular this data show an accumulation in FAPs from Old MDX mice.

## Discussion

Given their intrinsic ability to either support muscle regeneration or to contribute to fibro-adipogenic degeneration of diseased muscles, FAPs' fate choice has the potential to dramatically affect the outcome of skeletal muscle repair. FAPs have been described as, non-myogenic, bi-potent mesenchymal progenitors able to differentiate, *in vitro* and *in vivo*, into fibroblasts and adipocytes (Joe A.W., et al 2010; Uezumi A., et al 2010). Here, we unraveled the epigenetic silencing mechanism responsible to maintain repressed the myogenic program in FAPs. Our data identified G9a and GLP as H3K9 KMTs specifically enriched in FAPs, in which they mediate H3K9me2 deposition and silencing of key myogenic genes. In fact, G9a/GLP knock-down unlock the expression of key myogenic determination factors (i.e. Myf5, MyoD) in FAPs that consequently acquire the capacity to differentiate into mature myofibers *ex vivo*. Neither G9a nor GLP possess DNA-binding domains, meaning that they have to rely on binding partners to be targeted to specific genomic loci. Prdm16 has been identified recently as one factor able to recruit GLP to myogenic loci in Myf5<sup>+</sup> embryonic precursors (Ohno et al., 2013). PRDM family members are indeed defined by the presence of DNA- binding zinc-finger repeat that confers them the ability to directly bind DNA (Mozzetta et al., 2015). Of note, we show here that FAPs specifically express Prdm16 and we demonstrate that it interacts with GLP preferentially at the nuclear periphery. This observation, together with the evidence that H3K9me2 is mostly enriched beneath the nuclear lamina (NL), and that Prdm16 sharply co-localize with nuclear Lamin B, leads to the intriguing speculation that Prdm16 might serve as a specific NL-tethering factor to confine genomic regions that have to be maintained stably repressed at the nuclear periphery. NL is a well- known silent compartment of the nucleus

enriched in H3K9me2 (Guelen L. et al., 2008) where silenced chromatin is confined to prevent transcriptional activation. Lamina-Associated Domains (LADs), chromatin fragments (0.1–10 megabase in humans) enriched for lamina interactions, have been now mapped in different cell types. These chromatin fragments are generally expressed at a low level and are enriched in repressing histone marks, such as H3K9me2 and H3K27me3 (van Steensel and Belmont, 2017). Importantly, H3K9 methyltransferases have been implicated in mediating interactions between NL and chromatin (van Steensel and Belmont, 2017). In mammalian cells, disruption or inhibition of G9a weakened NL-LADs interactions (Kind et al., 2013) in line with our hypothesis that G9a-mediated H3K9me2 is important to confine silent chromatin to the nuclear periphery. Of note, we observed that Prdm16 depletion leads to defects in nuclear lamina architecture, as also reported in (Pinheiro et al., 2012), further supporting a role for these H3K9 KMTs in mediating heterochromatin formation and integrity. Moreover, the evidence that Prdm16-depleted FAPs show MyoD aneuploidy leads to speculate that Prdm16 might have a role in stabilizing chromatin interactions to the NL during cell cycle progression, as in its absence cells accumulate chromosomal aberrations. More importantly, these results highlight the importance to only block the enzymatic activities of the Prdm16 complex, that is G9a/GLP, in order to preserve nuclear integrity since A-366 inhibitor did not exert any aberration in nuclear structure.

Nonetheless, our results revealed a role for Prdm16-dependent H3K9 methylation as a mechanism to confine silent myogenic genes to the nuclear periphery. Whether these genes belong to LADs in FAPs is something that we plan to further investigate in the future. Nonetheless, our data identify a critical epigenetic axis that we think might be further exploited therapeutically. Indeed, the acquisition of the myogenic differentiation capacity upon inhibition

of Prdm16/G9a/GLP is accompanied by a decreased adipogenic differentiation, which is in line with previous studies reporting that these two differentiation programs are mutually exclusive to guarantee robustness and discreteness of cell fates (Sunadome et al., 2014). This evidence also suggests that strategies aimed to inhibit G9a/GLP activity might represent a way to reprogram FAPs fate towards myogenesis, thus blocking their adipogenic degeneration, with obvious beneficial implications in the context of muscle degenerative diseases characterized by fatty and fibrotic infiltrations, such as Duchenne Muscular Dystrophies (DMD). In agreement with this idea, our experiments performed using the G9a/GLP specific inhibitor A-366 indicate that FAPs fate can be indeed switched.

Taken together, our data identified an epigenetic axis of therapeutic relevance and candidate H3K9 KMTs as possible pharmacological targets to be used to enhance endogenous FAPs plasticity to promote regeneration and reverse pathologic plasticity observed in dystrophic muscles.

## Material and methods

### Animal Studies

For muscle regeneration experiments, mice were anesthetized, and muscle injury was induced by intra-muscular injection of Cardiotoxin (CTX, Laxotan) 20 µg/ml dissolved in saline solution.

For A-366 *in vivo* treatment, mice were treated for the indicated periods with daily intra-peritoneal injection of A-366 (2 mg/Kg), dissolved in 10% H-P-β Cyclodextrin in Citrate Buffer, or 10% H-P-β Cyclodextrin in Citrate Buffer alone (vehicle) as control. To perform Prdm16 conditional FAP-specific ablation *in vivo* we crossed PRDM16<sup>Flox/Flox</sup> with PDGFRA<sup>Cre-ERT/+</sup> mice. To conditionally induce Cre Recombinase, we intra-peritoneally injected tamoxifen (TMX-Sigma -80 mg/kg) for 5 consecutive days to 1,5 month old young adult PRDM16<sup>Flox/Flox</sup>:PDGFRA<sup>Cre-ERT/+</sup> double transgenic mice, and in PRDM16<sup>Flox/Flox</sup>:PDGFRA<sup>+/+</sup> mice, without the Cre (used as controls). After TMX injection, 5 days before the isolation of FAPs we induced skeletal muscle regeneration by CTX.

For Osr1 lineage tracing experiments, skeletal muscle regeneration was induced in the tibialis anterior (TA) of Osr1GCE/+;R26RmTmG/+ mice by intra-muscular injection of CTX at day 0, in concomitance to TMX (80 mg/kg) administration. Upon 2 consecutive days of TMX and 2 days of wash-out, a group of mice was then treated with 5 daily IP injections of A-366 (2 mg/kg), while another group with vehicle as control. Muscles were collected 10 d.p.i. Upon CreERT2 activation, the mTmG allele is

converted as to switch cells from membrane tomato (mT) expression to membrane eGFP (mG) expression.

For the experiment on MDX mice we use 1,5-month-old MDX mice as a model of young mice while 12-month-old as old mice. All mice were housed in accordance with standard procedures, and all experimental protocols were approved and conformed to the regulatory standards. All animals were kept in a temperature of 22°C (+2°C) with a humidity between 50% and 60%, in animal cages with at least 5 animals.

### **Cell preparation and FACS**

Cell isolation and labeling was essentially performed as described in Mozzetta et al, 2013. Briefly, whole lower hindlimb muscles were carefully isolated, minced and digested in PBS (Sigma) supplemented with 2.4 U/ml Dispase II (Roche), 100 µg/ml Collagenase A (Roche), 50 mM CaCl<sub>2</sub>, 1 M MgCl<sub>2</sub>, 10 mg/ml DNase I (Roche) for 1 h at 37 °C under agitation. Muscle slurries were passed 10 times through a 20G syringe (BD Bioscience). Cell suspension was obtained after three successive cell strainer filtrations with Washing Buffer (HBSS with 0.2% BSA (Sigma Aldrich), 1% penicillin-streptomycin). Cells were incubated with primary antibodies CD31-PE (MiltenyBiotec; 1:25), CD45- PE (MiltenyBiotec; 1:25), Ter119-PE (MiltenyBiotec; 1:25); Sca1-FITC or Sca1-APC (MiltenyBiotec 1:25); and α7Integrin-APCVio770 (MiltenyBiotec; 1:20) for 45 min on ice diluted in washing buffer + 1% DNase I. The suspension was finally washed and resuspended in PBS containing 2% Fetal Bovine Serum (FBS) and EDTA 0.5 µM. Muscle satellite cells (MuSCs) were isolated as Ter119<sup>neg</sup>/CD45<sup>neg</sup>/CD31<sup>neg</sup>/α7- integrin<sup>pos</sup>/Sca<sup>neg</sup>/GFP<sup>neg</sup> cells, while Fibro-Adipogenic Progenitors (FAPs) were isolated as

Ter119<sup>neg</sup>/CD45<sup>neg</sup>/CD31<sup>neg</sup>/a7integrin<sup>neg</sup>/Sca1<sup>pos</sup>/GFPP<sup>pos</sup>.

The FACS sorting analysis were performed on a FACS Aria II (BD Biosciences). Sorting gates were defined based on unstained controls. Data were collected using FACSDIVA software.

## Cell Culture

Freshly sorted cells were plated on 1mg/ml ECM Gel-coated dishes in Cyto-grow (Resnova) complete medium as a growth medium (GM). For adipogenic differentiation (DM) of FAPs, generally after 7 days of GM, cells were exposed for 3 days to adipogenic induction medium (DMEM, 10% FBS, 0.5 mM IBMX, 0.25 mM dexamethasone and 10 mg/ml insulin), followed by further 3 days in adipogenic maintenance medium (DMEM, 10% FBS and 10 mg/ml insulin). For A-366 *in vitro* treatment, cells were treated for 48h with 1nM A-366 in GM and then switched in adipogenic DM without the drug.

For the clonal analysis, FAPs<sup>Prdm16<sup>CKO</sup></sup> and FAPs<sup>ctr</sup> cells were directly plated as single cells onto 96 multiwell plates (Falcon) upon FACS isolation; and grown in Cyto-Grow (Resnova) complete medium for 23 days. Medium was changed every 72 h.

The WT-1 brown pre-adipocytes (Tseng et al., 2004) was gently donated to us by the Stricker Sigmar's laboratory. WT-1 were grown to confluence in DMEM+ 20% FBS. The HEK293T cells were grown in DMEM+ 10% FBS. All cells were cultured in incubator at 37 °C and 5% CO<sub>2</sub>.

## RNA interference

Downregulation of KMTs expression by siRNA mediated KD (Sigma), was performed by transfection with Lipofectamine 2000 (Invitrogen), according to the manufacturer's instructions, as

control (Scramble) we use Mission siRNA Universal Negative Control (Sigma). Sequences are detailed in table *Key Resources Table1* (see below).

## **Immunofluorescence**

For immunofluorescence on skeletal muscles, tibialis anterior muscles were excised and snap frozen in liquid nitrogen-cooled isopentane. For TA from PDGFRaGFP mice, muscles were prefixed in 4% paraformaldehyde (PFA) for 2 h at 4 °C and cryopreserved with 30% sucrose overnight at 4 °C. The day after, muscles were embedded in OCT compound (Sakura Finetek) and snap frozen in liquid nitrogen-cooled isopentane. Transverse cryosections (8µm), collected using a Leica CM 3050S cryostat, were fixed in 4% PFA for 20 min and permeabilized with 100% methanol for 6 min at -20 °C. To avoid unspecific binding, muscle sections were first blocked with a solution containing 4% BSA in PBS for 1 h at RT. Immunostaining with primary antibodies was performed overnight (O/N) at 4 °C. Antibody binding was revealed using species-specific secondary antibodies coupled to Alexa Fluor 488 or 594 (Thermo Fisher). Nuclei were visualized by counterstaining with DAPI (Sigma) in PBS. Primary antibodies used were against: Laminin (Sigma, 1:300), GFP (Abcam, 1:1000), eMyHC (DSHB 1:10). Images were acquired with a Nikon eclipse TE300 microscope and edited using the ImageJ. Images reported in the figures are representative of all examined fields.

For the immunofluorescence on FAPs, cells grown on ECM-coated coverslips were fixed with 4% paraformaldehyde in PBS for 20 min at RT, and permeabilized with 0.5% Triton X-100 in PBS, and unspecific signals were blocked with 4% BSA in PBS for 1 h at RT. Primary antibodies for GLP, G9a, H3K9me1, HeK9me2 HeK9me3

was diluted 1:500, while MyHC and Prdm16 was diluted 1:50, Lamin B and Perilipin was diluted 1:200, all of them were incubated O/N at 4°C. All primary antibodies were diluted in a PBS solution containing 4% BSA. Cells were stained with appropriate secondary antibodies coupled to Alexa Fluor 488 or 594 (Thermo Fisher), diluted 1:500, for 1 h at RT and washed in PBS. DNA was counterstained with DRAQ5 (Thermo Scientific) 1:1000 in PBS, or with DAPI (Sigma) in PBS and glasses were mounted in ProLong™ Diamond Antifade Mountant (Invitrogen). ImageJ was used to quantify the area occupied by Perilipin positive adipocytes.

### **PLA - Proximity Ligation Assay**

For PLA experiments on FAPs, coverslips were fixed with 4% paraformaldehyde in PBS for 20 min at RT. Cells were permeabilized with 0.5% Triton X-100 in PBS and blocked with 4% BSA in PBS for 1 h at RT. Detection of protein interactions was performed using the Duolink System (Sigma-Aldrich) according to the manufacturer's instructions.

### **DNA FISH**

Fluorescent in situ hybridization (FISH) was carried out on cells that adhered to glass coverslips coated with ECM Gel (Sigma) using nick-translated BAC DNA (BAC RP23-471- Myod Locus) which incorporate Cyanine 3-dUTP (Enzo Life Sciences). Three-dimensional (3D) DNA FISH on FAPs was performed with some modifications of an already described procedure (Cremer et al, 2008). Briefly, cells were fixed in 4% PFA (20 min at 4°C) and pre-processed by freeze-thawing permeabilization to ensure the preservation of nuclear structures. After denaturation, FISH probes were hybridized O.N. at 37°C and samples washed, DAPI-stained,

and mounted in ProLong Diamond reagent (Thermo Fisher Scientific). Samples were imaged on inverted microscope (Olympus IX73) equipped with a Confocal Imager (CREST X-LIGHT) spinning disk, a CoolSNAP MYO CCD camera (Photometrics), and a Lumencor Spectra X LED illumination. Images were acquired with 60× NA1.35 oil objective (UPLANSApo) and MetaMorph (Molecular Devices) using 300 (Cy3), 300 (Fluorescein), or 100 (DAPI) ms as exposure time. Confocal images were taken with a 0,2 um step Z stacks. 3D reconstructions and 3D-distance between the center of mass of the DNA-FISH spots and the inner surface of the lamina were performed by using Huygens Professional software.

## **RT-PCR**

Total RNA was extracted with TriReagent (Sigma), and 0.5–1ug were retro-transcribed using the High Capacity reverse transcription kit (Applied Biosystems). Quantitative RT-PCR (qRT-PCR) was performed on a Step-one plus instrument (Applied Biosystem) using SYBR Green Master mix (Applied Biosystems) following manufacturer indications. qRT-PCR data were analysed according to the 2-ddCT method using GAPDH levels as a reference control gene. Data are presented as mean of log<sub>2</sub>-fold changes.

Primers sequences used in this study are:

### **mPparg:**

Fw: 5'-CGCTGATGCACTGCCTATGA-3'

Rev: 5'-AGAGGTCCACAGAGCTGATTCC-3'

**mMyf5:**

Fw: 5'-CAG CCC CAC CTC CAA CTG-3'

Rev: 5'-GGG ACC AGA CAG GGC TGT TA-3'

**mPlin1:**

Fw: 5'-GGCCTGGACGACAAAACC-3'

Rev: 5'-CAGGATGGGCTCCATGAC-3'

**mGAPDH:**

Fw: 5'-CACCATCTTCCAGGAGCGAG-3'

Rev: 5'-CCTTCTCCATGGTGGTGAAGAC-3'

**mMyHC3 RT (MHC embryonic):**

Fw: 5'-CAATAAACTGCGGGCAAAGAC 3'

Rev: 5'-CTTGCTCACTCCTCGCTTTCA 3'

**mMyHC8 RT (MHC perinatal):**

Fw: 5'-GAACTTGAAGGAGAGGTCGA 3'

Rev: 5'-GAGCACATTCTTGCGGTCTT 3'

**mMyoD:**

Fw: 5'-CGCGCTCCAAGTCTGATGG-3'

Rev: 5'-CTCGACACAGCCGCACTCTTCC-3'

**mCebpa:**

Fw: 5'- GCCGAGATAAAGCCAAACAAC -3'

Rev:5'- GACCCGAAACCATCCTCTG -3'

**mAP2 (Fabp4):**

Fw: 5'-ACA CCG AGA TTT CCT TCA AAC TG -3'

Rev: 5'-CCA TCT AGG GTT ATG ATG CTC TTCA-3'

### **mAdiponectin (Adipoq)**

Fw: 5'-GCCGTTCTCTTCACCTACGA -3'

Rev: 5'-ACTTGGTCTCCACCTCCA-3'

### **mDesmin-DES**

Fw: 5'-AACTTCCGAGAAACCAGCCC-3'

Rev: 5'-CTGTGTAGCCTCGCTGACAA-3'

### **Cell Lysis and Immunoblot**

Total proteins were prepared by resuspending cells in RIPA buffer (50mM Tris-HCl pH 7.4, 150mM NaCl, 0.1% SDS, 0.5% sodium deoxycholate, 1% NP-40, 1mM EDTA, protease and phosphatase inhibitors (Roche)). Protein concentration was determined using a BCA assay (Thermo Fisher Scientific). The cell lysate was denatured at 95 °C for 5 min. The cell lysates were resolved on 4%–15% TGX gradient gels (Bio-Rad Laboratories) and transferred to nitrocellulose membrane (Amersham). Membranes were blocked with 5% non-fat dried milk in TBS with 0.2% Tween for 1 h at RT, and then incubated with primary antibody overnight at 4°C. Primary antibodies used were: PAX7 and MF20 (1:20), Prdm16 (1:200), GLP, PDGFRa, aSMA and H3K9me2 (1:500), G9a, SETDB1, SUV39h1, H3K9me1, HeK9me3, H3 Total, LaminB and Lamin A/C (1:1000); GAPDH and Tubulin diluted 1:5000. After washing in TBS with 0.2% Tween, membranes were incubated with species-specific HRP-conjugated secondary antibodies for 1h at RT. After washing in TBS with 0.2% Tween, blots were developed with Western lightning enhanced chemiluminescence (Thermo Fisher Scientific) and signal detected with ChemiDoc (BioRad). Quantification of protein expression levels was performed using

GAPDH/Tubulin protein level as a reference using the Image Lab 6.0 software (BioRad).

### **Chromatin fractionation**

FAPs were washed in PBS and extracted in cytoskeleton (CSK) buffer (10 mM Pipes, pH 6.8, 100 mM NaCl, 1 mM EGTA, 300 mM sucrose, 3 mM MgCl<sub>2</sub>, protease inhibitors, and 1 mM PMSF supplemented with 1 mM DTT and 0.5% Triton X-100). After 5 min at 4 °C, the cytoskeletal fraction was separated from soluble proteins by centrifugation at 3,000 rpm for 3 min, and the supernatant was designated the S1 fraction. The pellets were washed with an additional volume of CSK buffer. Chromatin was solubilized by DNA digestion with 25 U RNase-free DNase (Invitrogen) in CSK buffer for 30 min at 37°C. Ammonium sulfate was added in CSK buffer to a final concentration of 250 mM. After 5 min at 4°C, samples were pelleted again at 5,000 rpm for 3 min at 4 °C, and the supernatant was designated as S2 fraction. After a wash in CSK buffer, the pellet was further extracted with 2M NaCl in CSK buffer for 5 min at 4°C and centrifuged at 5,000 rpm for 3 min at 4 °C; the supernatant was designated as S3 fraction. This treatment removed all the DNA and histones from the nucleus, as shown by SDS-PAGE. After two washes in NaCl 2M CSK, the insoluble pellets were solubilized in 8M urea buffer and were considered the nuclear matrix-containing fraction (S4). Supernatants from each extraction step were quantified and analyzed by SDS-PAGE and immunoblotting.

### **ChIP**

For ChIP analysis the DNA was crosslinked to proteins with and 1% Formaldehyde (Sigma). After incubation for 15 min at RT in

gently agitation, glycine was added to a final concentration of 0.125 M for 5 min. The cells were washed twice with cooled PBS, scraped and pelleted. Chromatin was prepared by two subsequent extraction steps (10 min, 4 °C) with: Buffer 1 (50 mM HEPES/KOH pH 7.5; 140 mM NaCl; 1 mM EDTA; 10% Glycerol; 0.5% NP-40; 0.25% Triton) and Buffer 2 (200 mM NaCl; 1mM EDTA; 0.5 mM EGTA; 10 mM Tris pH 8). Nuclei were then pelleted by centrifugation, resuspended in Buffer 3 (50 mM Tris pH 8; 0.1% SDS; 1% NP-40; 0.1% Na- Deoxycholate; 10 mM EDTA; 150 mM NaCl) and subjected to sonication with Bioruptor Power-up (Diagenode) yielding genomic DNA fragments with a bulk size of 150-300 bp. Chromatin was precleared with Protein A/G Magnetic beads (Thermo Scientific) for 2h at 4°C and immunoprecipitation with the specific antibodies carried out overnight at 4 °C. Beads were then added for 2h to recover DNA-protein complexes and then washed twice with Low salt buffer (0.1% SDS; 1% Triton; 2 mM EDTA; 20 mM Tris pH 8; 150 mM NaCl), twice with High salt buffer (0.1% SDS; 1% Triton; 2 mM EDTA; 20 mM Tris pH 8; 500 mM NaCl), once with LiCl wash buffer (10 mM Tris pH 8.0; 1% Na-deoxycholate; 1% NP- 40, 250 mM LiCl; 1 mM EDTA) and twice with TE + 50 mM NaCl. Beads were then eluted in TE + 1% SDS at 65°C and cross- linking was reversed O/N at 65°C in the presence of RNase. The eluted material was treated with Proteinase K for 2h and then phenol/chloroform-extracted and ethanol- precipitated. DNA was resuspended in water and q-PCR performed using Power up SYBR Green PCR Master mix (Applied Biosystems) and analyzed on Step-one plus real time PCR (Applied Biosystems). ChIP-qPCR results were represented as percentage of IP/input signal (% input).

ChIP primers sequences:

**MyoD TSS:**

Fw: AGATAGCCAAGTGCTACCGC

Rev: CCAGGGTAGCCTAAAAGCCC

**MyoD CE:**

Fw: CTAAACACCAGGCATGAGAGG

Rev: ACTCACTTTCTCCCAGAGTTGC

**Des:**

Fw: GGTGATGTCAGGAGGGCTAC

Rev: GGCTGGAGTGGATGTGAAGA

**Ap2:**

Fw: GAGGGTGCTATGAGCCTCTG

Rev: ACAGGGTCTGGTCATGAAGG

**Fn1:**

Fw: CCTCCCTCCAGACTTTACCC

Rev: GGAGGGGTGGATAGTGAAT

**Ctrl+ (R15):**

Fw: GTTTTTCATCGGACGGTGGC

Rev: CCGCCGCTCATACACCATAA

**Ctrl- (Ube2b prom):**

Fw: GCCGAACTTGAAACTAGCGAC

Rev: GTTGCTTGCGGGCAACTACG

## **Quantification and statistical analysis**

The images were taken with optical microscope (Nikon), or with confocal microscope (Zeiss). The Perilipin positive droplets was measured using ImageJ, calculating the area of the red pixels (pixel<sup>2</sup>) per field. For western blot analysis quantification, images from ChemiDoc are analyzed by Image Lab software and, using the quantification tool, to obtain densitometry for lanes and bands.

The statistical details of experiments can be found in the figure legends. All data are represented as mean  $\pm$  standard error of the mean (s.e.m). Graphs were created with Graphpad Prism 8, which was used for all statistical tests. The number of replicates (n) and the statistical test applied for each experiment is indicated in the figure legends. Differences were considered statistically different at  $p < 0.05$ .

## Key Resources Table

REAGENT or RESOURCE	SOURCE	IDENTIFIER CODE
<b>Antibodies</b>		
ANTI MOUSE Ly-6A E (SCA-1) FITC	MILTENYIBIOT EC	130-116-490
ANTI-MOUSE CD45 PE	MILTENYIBIOT EC	130-110-707
ANTI-MOUSE TER-119 PE	MILTENYIBIOT EC	130-112-909
ANTI-MOUSE CD31 (PECAM-1) PE	MILTENYIBIOT EC	130-111-540
ANTI-INTEGRIN ALPHA7 APC VIO770	MILTENYIBIOT EC	130102719
ANTI-LAMININ	SIGMA	L9393
ANTI-PERILIPIN	SIGMA	P1873
ANTI-MYHC1	DSHB	Mf20-s
ANTI-HISTONE H3	ABCAM	AB1791
ANTI- HISTONE H3 DYMETIL K9	ABCAM	AB1220
ANTI- HISTONE H3 DYMETIL K9	ACTIVE MOTIF	39293
ANTI-HISTONE H3 MONOMETIL	ACTIVE MOTIF	39887
ANTI-HISTONE H3 TRIMETIL	ACTIVE MOTIF	39161
ANTI-ACETYL-H3	ABCAM	AB10812
ANTI-GLP	ABCAM	AB41969
ANTI-G9a	ABCAM	AB185050
ANTI-PRDM16	R&D	AF6295
ANTI SMA	SANTA CRUZ	SC-53015

ANTI GAPDH	SIGMA	G9545
ANTI-GFP	ABCAM	AB13970
ANTI-LAMIN B1	ABCAM	AB16048
ANTI-LAMIN B1 (B-10)	SANTA CRUZ	SC-374015
SUV39H1(44.1)	SANTA CRUZ	SC-23961
ESET(A-1)	SANTA CRUZ	SC-166621
GFP	ABCAM	AB13970
ALEXA ANTI RABBIT 488	THERMO FISHER	A21206
ALEXA ANTI MOUSE 488	THERMO FISHER	A21202
ALEXA ANTI RABBIT 594	THERMO FISHER	A21207
ALEXA ANTI MOUSE 594	THERMO FISHER	A21203
ANTI-CHICKEN 488	SIGMA	SAB460005 2
ANTI-SHEEP IgG	SIGMA	A3415
ANTI-RABBIT IgG	SIGMA	A9169
ANTI-MOUSE IgG	SIGMA	A9044
<b>Chemicals, Peptides, and Recombinant Proteins</b>		
POWER UP SYBR Green 2X master mix	APPLIED BIOSYSTEMS	4367659
COLLAGENASE A	ROCHE	1010358600 1
Dispase II	ROCHE	04 942 078 001
DNase I	ROCHE	1284932
TAMOXIFEN	SIGMA	T5648

CARDIOTOXIN	LAXOTAN	L8102
LIPOFECTAMNIE 2000	INVITROGEN	11668019
DMEM	SIGMA	D5671
HBSS, W/O PHENOL RED	GIBCO	14025100
FBS, CERT, USA ORIGIN	GIBCO	16000044
HORSE SERUM HEAT INACTIVATED	GIBCO	26050088
GLUTAMAX	GIBCO	35050-061
INSULIN	SIGMA	19278
DEXAMETAZONE	SIGMA	D4902
IBMX	SIGMA	15879
CYTOGROW	RESNOVA	9001-B
ECM	SIGMA	E1270
<b>REAGENT or RESOURCE</b>		
4%-15% TGX gradient gels	BIO-RAD	456-1086
Nitrocellulose Membrane	AMERSHAM	10600016
SUPER SIGNAL WEST DURA	THERMO FISHER	34075
BCA PIERCE KIT	THERMO FISHER	23225
Hight capacity cDNA reverse transcription Kits	APPLIED BIOSYSTEMS	4368813

ProLong™ Diamond Antifade Mountant	INVITROGEN	p36970
DAPI	SIGMA	D9542
DRAQ5 fluorescent Probe	THERMO FISHER	62254
TriReagent	SIGMA	T9424
ZOLETIL 50/50 MG	VIRBAC	101580025
ROMPUN 20 MG/ML-SOLUTION	BAYERN	100390018
Complete Protease Inhibitors Tablets	ROCHE	0-4693116001
(2-Hydroxypropyl)- $\beta$ -cyclodextrin POWDER	SIGMA	H107
<b>Experimental Models: Organisms/Strains</b>		
C57/BL6J MICE	JACKSON LABORATORY	
C57BL/10ScSn- <i>Dmd</i> <sup>tm1dx</sup> /J	JACKSON LABORATORY	
B6.129S4-Pdgfra <sup>tm11(EGFP)Sor/J</sup>	JACKSON LABORATORY	007669
B6.129-Prdm16 <sup>tm1.1Brsp/J</sup>	JACKSON LABORATORY	024992
B6N.Cg-Tg(PDGFR <sup>acre</sup> /ERT)467 Dbe/J	JACKSON LABORATORY	018280
<b>Oligonucleotides</b>		
Mission siRNA Universal Negative Control	SIGMA	1152
SiPRDM16	SIGMA	SASI_Mm01_00154717
SiPRDM16	SIGMA	SASI_Mm01_00154718

SiPRDM16	SIGMA	SASI_Mm01_00154719
SiGLP	SIGMA	SASI_Mm01_001090079
SiGLP	SIGMA	SASI_Mm01_001090080
SiGLP	SIGMA	SASI_Mm01_001090081
SiG9a	SIGMA	SASI_Mm01_001090074
SiG9a	SIGMA	SASI_Mm01_001090075
<b>Critical Commercial Assays</b>		
PLA	SIGMA	DUO92004 mouse minus
PLA	SIGMA	DUO92009 rabbit plus
DUOLINK in situ detection reagent green	SIGMA	DUO92014
<b>Software and Algorithms</b>		
Image Lab 6.0	BIO-RAD	
Prism	GMSL	
ImageJ	NIH	
FACS DIVA	BD BIOSCIENCES	
<b>Other</b>		
CHEMIDOC	BIORAD	XRS+
CRYOSTAT	LEICA	CM-3050 S
MICROSCOPE	NIKON	eclipse TE300
CONFOCAL MICROSCOPE	ZEISS	
Bioruptor Power-up	DIAGENODE	
FACS Aria II	BD Biosciences	

## References

Brack, A.S., and Rando, T.A. (2012). Tissue-specific stem cells: lessons from the skeletal muscle satellite cell. *Cell stem cell* *10*, 504-514.

Wang, Y.X., Bentzinger, C.F., and Rudnicki, M.A. (2013). Molecular regulation of determination in asymmetrically dividing muscle stem cells. *Cell cycle* *12*, 3-4.

Lepper, C., Partridge, T.A., and Fan, C.M. (2011). An absolute requirement for Pax7-positive satellite cells in acute injury-induced skeletal muscle regeneration. *Development* *138*, 3639-3646.

Murphy, M.M., Lawson, J.A., Mathew, S.J., Hutcheson, D.A., and Kardon, G. (2011). Satellite cells, connective tissue fibroblasts and their interactions are crucial for muscle regeneration. *Development* *138*, 3625-3637.

Sambasivan, R., Yao, R., Kissenpfennig, A., Van Wittenberghe, L., Paldi, A., Gayraud-Morel, B., Guenou, H., Malissen, B., Tajbakhsh, S., and Galy, A. (2011). Pax7-expressing satellite cells are indispensable for adult skeletal muscle regeneration. *Development* *138*, 3647-3656.

Wosczyzna, M.N., and Rando, T.A. (2018). A Muscle Stem Cell Support Group: Coordinated Cellular Responses in Muscle Regeneration. *Dev Cell* *46*, 135-143.

Wosczyzna, M.N., Konishi, C.T., Perez Carbajal, E.E., Wang, T.T., Walsh, R.A., Gan, Q., Wagner, M.W., and Rando, T.A. (2019). Mesenchymal Stromal Cells Are Required for Regeneration and

Homeostatic Maintenance of Skeletal Muscle. *Cell Rep* 27, 2029-2035 e2025.

Joe, A.W., Yi, L., Natarajan, A., Le Grand, F., So, L., Wang, J., Rudnicki, M.A., and Rossi, F.M. (2010). Muscle injury activates resident fibro/adipogenic progenitors that facilitate myogenesis. *Nature cell biology* 12, 153-163.

Uezumi, A., Fukada, S., Yamamoto, N., Takeda, S., and Tsuchida, K. (2010). Mesenchymal progenitors distinct from satellite cells contribute to ectopic fat cell formation in skeletal muscle. *Nat Cell Biol* 12, 143-152.

Heredia, J.E., Mukundan, L., Chen, F.M., Mueller, A.A., Deo, R.C., Locksley, R.M., Rando, T.A., and Chawla, A. (2013). Type 2 innate signals stimulate fibro/adipogenic progenitors to facilitate muscle regeneration. *Cell* 153, 376-388.

Lemos, D.R., Babaeijandaghi, F., Low, M., Chang, C.K., Lee, S.T., Fiore, D., Zhang, R.H., Natarajan, A., Nedospasov, S.A., and Rossi, F.M. (2015). Nilotinib reduces muscle fibrosis in chronic muscle injury by promoting TNF-mediated apoptosis of fibro/adipogenic progenitors. *Nat Med* 21, 786-794.

Lukjanenko, L., Karaz, S., Stuelsatz, P., Gurriaran-Rodriguez, U., Michaud, J., Dammeone, G., et al. (2019). Aging Disrupts Muscle Stem Cell Function by Impairing Matricellular WISP1 Secretion from Fibro-Adipogenic Progenitors. *Cell Stem Cell* 24, 433–446.e7.

Mozzetta, C., Consalvi, S., Saccone, V., Tierney, M., Diamantini, A., Mitchell, K.J., Marazzi, G., Borsellino, G., Battistini, L.,

Sassoon, D., *et al.* (2013). Fibroadipogenic progenitors mediate the ability of HDAC inhibitors to promote regeneration in dystrophic muscles of young, but not old Mdx mice. *EMBO molecular medicine* 5, 626-639.

Kopinke, D., Roberson, E.C., and Reiter, J.F. (2017). Ciliary Hedgehog Signaling Restricts Injury- Induced Adipogenesis. *Cell* 170, 340-351 e312.

Uezumi, A., Ito, T., Morikawa, D., Shimizu, N., Yoneda, T., Segawa, M., Yamaguchi, M., Ogawa, R., Matev, M.M., Miyago-Suzuki, Y., *et al.* (2011). Fibrosis and adipogenesis originate from a common mesenchymal progenitor in skeletal muscle. *Journal of cell science* 124, 3654-3664.

Lees-Shepard, J.B., Yamamoto, M., Biswas, A.A., Stoessel, S.J., Nicholas, S.E., Cogswell, C.A., Devarakonda, P.M., Schneider, M.J., Jr., Cummins, S.M., Legendre, N.P., *et al.* (2018). Activin-dependent signaling in fibro/adipogenic progenitors causes fibrodysplasia ossificans progressiva. *Nat Commun* 9, 471.

Saccone, V., Consalvi, S., Giordani, L., Mozzetta, C., Barozzi, I., Sandona, M., Ryan, T., Rojas-Munoz, A., Madaro, L., Fasanaro, P., *et al.* (2014). HDAC-regulated myomiRs control BAF60 variant exchange and direct the functional phenotype of fibro-adipogenic progenitors in dystrophic muscles. *Genes Dev* 28, 841-857.

Taddei, A., Maison, C., Roche, D., and Almouzni, G. (2001). Reversible disruption of pericentric heterochromatin and centromere function by inhibiting deacetylases. *Nature cell biology* 3, 114-120.

Mozzetta, C., Boyarchuk, E., Pontis, J., and Ait-Si-Ali, S. (2015). Sound of silence: the properties and functions of repressive Lys methyltransferases. *Nat Rev Mol Cell Biol* 16, 499-513.

Ait-Si-Ali, S., Guasconi, V., Fritsch, L., Yahi, H., Sekhri, R., Naguibneva, I., Robin, P., Cabon, F., Poleskaya, A., and Harel-Bellan, A. (2004). A Suv39h-dependent mechanism for silencing S-phase genes in differentiating but not in cycling cells. *Embo J* 23, 605-615.

Guasconi, V., Pritchard, L.L., Fritsch, L., Mesner, L.D., Francastel, C., Harel-Bellan, A., and Ait-Si-Ali, S. (2010). Preferential association of irreversibly silenced E2F-target genes with pericentromeric heterochromatin in differentiated muscle cells. *Epigenetics* 5, 704-9.

Mal, A.K. (2006). Histone methyltransferase Suv39h1 represses MyoDstimulated myogenic differentiation. *EMBO J.* 25, 3323–3334

Zhang, C.L., McKinsey, T.A., and Olson, E.N. (2002). Association of class II histone deacetylases with heterochromatin protein 1: potential role for histone methylation in control of muscle differentiation. *Mol Cell Biol* 22, 7302-7312.

Beyer, S., Pontis, J., Schirwis, E., Battisti, V., Rudolf, A., Le Grand, F., and Ait-Si-Ali, S. (2016). Canonical Wnt signalling regulates nuclear export of Setdb1 during skeletal muscle terminal differentiation. *Cell Discov* 2, 16037.

Shinkai Y., Tachibana M. (2011) H3K9 methyltransferase G9a and the related molecule GLP. *Genes Dev.* 25, 781-8.

Ling, B.M., Bharathy, N., Chung, T.K., Kok, W.K., Li, S., Tan, Y.H., Rao, V.K., Gopinadhan, S., Sartorelli, V., Walsh, M.J., *et al.* (2012a). Lysine methyltransferase G9a methylates the transcription factor MyoD and regulates skeletal muscle differentiation. *Proceedings of the National Academy of Sciences of the United States of America* *109*, 841-846.

Choi, J., Jang, H., Kim, H., Lee, J.H., Kim, S.T., Cho, E.J., and Youn, H.D. (2014). Modulation of lysine methylation in myocyte enhancer factor 2 during skeletal muscle cell differentiation. *Nucleic acids research* *42*, 224-234.

Puri, P.L., and Sartorelli, V. (2000). Regulation of muscle regulatory factors by DNA-binding, interacting proteins, and post-transcriptional modifications. *J Cell Physiol* *185*, 155-173.

Ohno, H., Shinoda, K., Ohyama, K., Sharp, L.Z., and Kajimura, S. (2013). EHMT1 controls brown adipose cell fate and thermogenesis through the PRDM16 complex. *Nature* *504*, 163-167.

Seale, P., Bjork, B., Yang, W., Kajimura, S., Chin, S., Kuang, S., Scime, A., Devarakonda, S., Conroe, H.M., Erdjument-Bromage, H., *et al.* (2008). PRDM16 controls a brown fat/skeletal muscle switch. *Nature* *454*, 961-967.

Aguilo, F., Avagyan, S., Labar, A., Sevilla, A., Lee, D.F., Kumar, P., Lemischka, I.R., Zhou, B.Y., and Snoeck, H.W. (2011). Prdm16 is a physiologic regulator of hematopoietic stem cells. *Blood* *117*, 5057-5066.

Chuikov, S., Levi, B.P., Smith, M.L., and Morrison, S.J. (2010). Prdm16 promotes stem cell maintenance in multiple tissues, partly by regulating oxidative stress. *Nat Cell Biol* *12*, 999-1006.

Inoue, M., Iwai, R., Tabata, H., Konno, D., Komabayashi-Suzuki, M., Watanabe, C., Iwanari, H., Mochizuki, Y., Hamakubo, T., Matsuzaki, F., *et al.* (2017). Prdm16 is crucial for progression of the multipolar phase during neural differentiation of the developing neocortex. *Development* *144*, 385-399.

Shimada, I.S., Acar, M., Burgess, R.J., Zhao, Z., and Morrison, S.J. (2017). Prdm16 is required for the maintenance of neural stem cells in the postnatal forebrain and their differentiation into ependymal cells. *Genes & development* *31*, 1134-1146.

Stine, R.R., Sakers, A.P., TeSlaa, T., Kissig, M., Stine, Z.E., Kwon, C.W., Cheng, L., Lim, H.W., Kaestner, K.H., Rabinowitz, J.D., *et al.* (2019). PRDM16 Maintains Homeostasis of the Intestinal Epithelium by Controlling Region-Specific Metabolism. *Cell Stem Cell*.

Pinheiro, I., Margueron, R., Shukeir, N., Eisold, M., Fritsch, C., Richter, F.M., Mittler, G., Genoud, C., Goyama, S., Kurokawa, M., *et al.* (2012). Prdm3 and Prdm16 are H3K9me1 methyltransferases required for mammalian heterochromatin integrity. *Cell* *150*, 948-960.

Gonzalez-Sandoval, A., Towbin, B.D., Kalck, V., Cebianca, D.S., Gaidatzis, D., Hauer, M.H., Geng, L., Wang, L., Yang, T., Wang, X., *et al.* (2015). Perinuclear Anchoring of H3K9-Methylated Chromatin Stabilizes Induced Cell Fate in *C. elegans* Embryos. *Cell* *163*, 1333-1347.

Tseng Y.H., Kriauciunas K.M., Kokkotou E., Kahn C.R. (2004) Differential roles of insulin receptor substrates in brown adipocyte differentiation. *Mol Cell Biol* 1918-29.

Poleshko A., Shah P.P., Gupta M., Babu A., Morley M.P., Manderfield L.J., Ifkovits J.L., Calderon D., Aghajanian H., Sierra-Pagán J.E., Sun Z, Wang Q., Li L., Dubois N.C., Morrissey E.E., Lazar M.A., Smith C.L., Epstein J.A., Jain R. (2017). Genome-Nuclear Lamina Interactions Regulate Cardiac Stem Cell Lineage Restriction. *Cell*. 171, 573-587.e14.

Kind, J., Pagie, L., Ortabozkoyun, H., Boyle, S., de Vries, S.S., Janssen, H., Amendola, M., Nolen, L.D., Bickmore, W.A., and van Steensel, B. (2013). Single-cell dynamics of genome-nuclear lamina interactions. *Cell* 153, 178-192.

Towbin, B.D., Gonzalez-Aguilera, C., Sack, R., Gaidatzis, D., Kalck, V., Meister, P., Askjaer, P., and Gasser, S.M. (2012). Step-wise methylation of histone H3K9 positions heterochromatin at the nuclear periphery. *Cell* 150, 934-947.

Pappano, W.N., Guo, J., He, Y., Ferguson, D., Jagadeeswaran, S., Osterling, D.J., Gao, W., Spence, J.K., Pliushchev, M., Sweis, R.F., *et al.* (2015). The Histone Methyltransferase Inhibitor A-366 Uncovers a Role for G9a/GLP in the Epigenetics of Leukemia. *PLoS One* 10, e0131716.

Guelen L., Pagie L., Brasset E., Meuleman W., Faza M.B., Talhout W., Eussen B.H., de Klein A., Wessels L., de Laat W., van Steensel B. (2008). Domain organization of human chromosomes revealed by mapping of nuclear lamina interactions. *Nature*. 453, 948-51.

Lund, E., Oldenburg, A.R., Delbarre, E., Freberg, C.T., Duband-Goulet, I., Eskeland, R., Buendia, B., and Collas, P. (2013). Lamin A/C-promoter interactions specify chromatin state-dependent transcription outcomes. *Genome Res* 23, 1580-1589.

Peric-Hupkes, D., Meuleman, W., Pagie, L., Bruggeman, S.W., Solovei, I., Brugman, W., Graf, S., Flicek, P., Kerkhoven, R.M., van Lohuizen, M., et al. (2010). Molecular maps of the reorganization of genome-nuclear lamina interactions during differentiation. *Mol Cell* 38, 603-613.

Tabula Muris, C., Overall, c., Logistical, c., Organ, c., processing, Library, p., sequencing, Computational data, a., Cell type, a., Writing, g., et al. (2018). Single-cell transcriptomics of 20 mouse organs creates a Tabula Muris. *Nature* 562, 367-372.

Vallecillo-García P., Orgeur M., Vom Hofe-Schneider S., Stumm J., Kappert V., Ibrahim D.M., Börno S.T., Hayashi S., Relaix F., Hildebrandt K., Sengle G., Koch M., Timmermann B., Marazzi G., Sassoon D.A., Duprez D., Stricker S. (2017). Odd skipped-related 1 identifies a population of embryonic fibro-adipogenic progenitors regulating myogenesis during limb development. *Nat Commun.* 8(1):1218.

Stumm J., Vallecillo-García P., Vom Hofe-Schneider S., Ollitault D., Schrewe H., Economides A.N., Marazzi G., Sassoon D.A., Stricker S. (2018) Odd skipped-related 1 (*Osr1*) identifies muscle-interstitial fibro-adipogenic progenitors (FAPs) activated by acute injury. *Stem Cell Res.* 32:8-16.

Hoffman EP1, Brown RH Jr, Kunkel LM. (1987). Dystrophin: the protein product of the Duchenne muscular dystrophy locus. *Cell*. 51, 919-28.

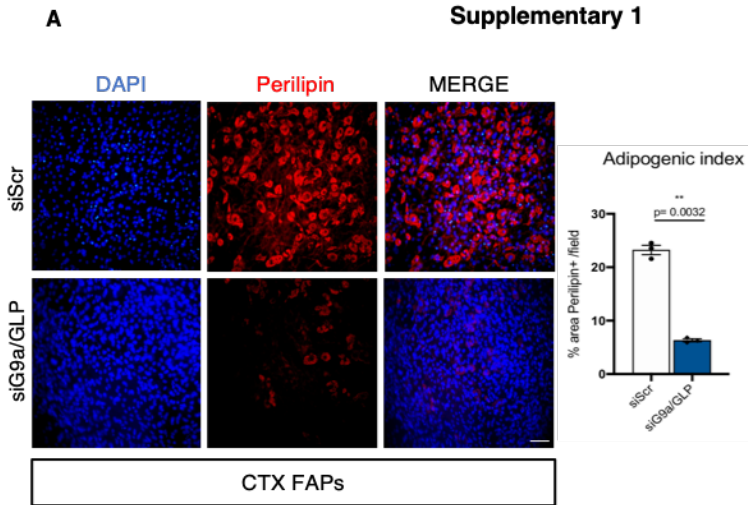
Van Steensel, B., and Belmont, A.S. (2017). Lamina-Associated Domains: Links with Chromosome Architecture, Heterochromatin, and Gene Repression. *Cell* 169, 780-791.

Sunadome, K., Suzuki, T., Usui, M., Ashida, Y., and Nishida, E. (2014). Antagonism between the master regulators of differentiation ensures the discreteness and robustness of cell fates. *Mol Cell* 54, 526-535

Kubben N. and Misteli T. (2017). Shared molecular and cellular mechanisms of premature ageing and ageing-associated diseases. *Nat Rev Mol Cell Bio*. 18(10):595-609

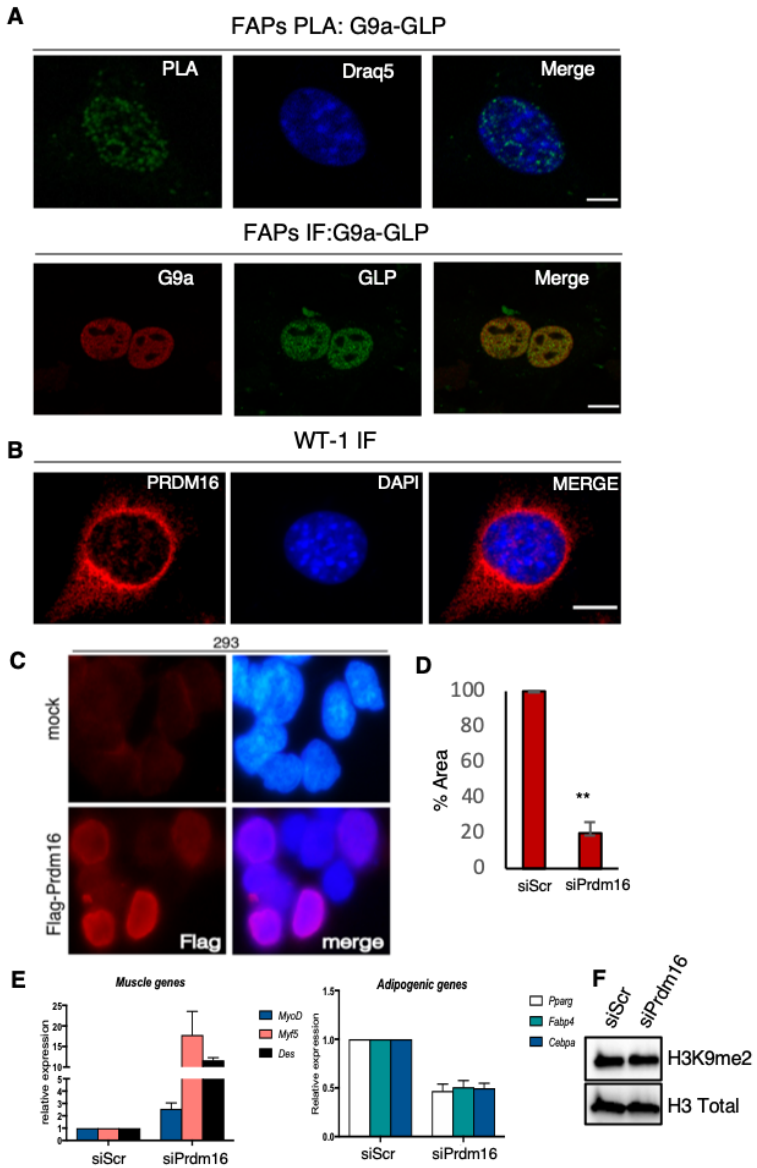
Biferali B., Proietti D., Mozzetta C., Madaro L. (2019) Fibro-Adipogenic Progenitors Cross-Talk in Skeletal Muscle: The Social Network. *Front Physiol* 10:1074.

## Supplementary Figures



### Supplementary 1: *SiG9a/GLP* induces a reduction of adipogenic differentiation in FAPs

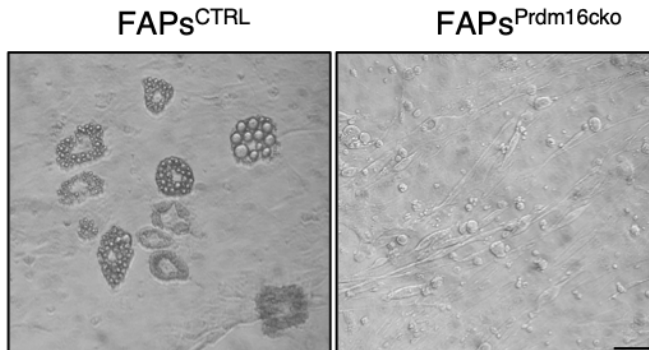
*A*) Representative images of immunofluorescence Perilipin (red) in differentiating FAPs from injured mice, cultured in adipogenic differentiation media after *G9a/GLP* KD (*siG9a/GLP*), as compared to control FAPs (*siScr*). Nuclei were counterstained with DAPI (blue). Scale bar: 100 $\mu$ m. Graph showing the quantification of the adipogenic differentiation of FAPs in the experiment represented in the panel. We measured the percentage of the Perilipin positive cells per field. The quantification results are the mean of three independent experiments ( $\pm$ S.D.) Statistical significance assessed by t-test,  $**p < 0.01$ .



## Supplementary 2: Prdm16 colocalize with the NL and the Prdm16 KD enhanced the myogenic switch of FAPs

**A)** Representative confocal microscopy images of FAPs and relative immunofluorescence (IF) for GLP and G9a as control for PLA experiment. Scale bar: 5 $\mu$ m **B)** Representative images of immunofluorescence for Prdm16 (red) in WT-1. Nuclei are counterstained with DAPI. Scale bar: 10  $\mu$ m. **C)** Representative images of immunofluorescence for FLAG (red) in HEK293T overexpressing Flag-Prdm16 versus Mock used as Ctrl. Nuclei are counterstained with DAPI. **D)** Graph showing the quantification of the adipogenic differentiation of FAPs in the experiment represented in the panel. We measured the percentage of the Perilipin positive cells per field. The quantification results are the mean of three independent experiments ( $\pm$ S.D.) (\*  $p<0.05$ ; \*\*  $p<0.01$ ; \*\*\*  $p<0.001$ ; \*\*\*\*  $p<0.0001$ ). **E)** qRT-PCR analysis of myogenic markers (*Myf5*, *MyoD*, *Des*) and adipogenic markers (*Pparg*, *Fabp4*, *Cebpa*) confirm that Prdm16 KD (*siPrdm16*) leads to reduced expression of adipogenic genes and enhanced transcription of key genes involved in muscle commitment. **F)** Western blot analysis revealed that FAPs after Prdm16 KD (*siPrdm16*) express the same levels of H3K9me2 compared to CTRL cells (*siScr*).

## Supplementary 3



### Supplementary 3: Clonal analysis

**A)** Representative phase contrast images showing a fibro-adipogenic clones (in FAPs<sup>Ctrl</sup>) and a myogenic clone (in FAPs<sup>Prdm16cko</sup>). Scale bar: 100 $\mu$ m.

## **Glossary**

FAPs: Fibro-Adipogenic Progenitors

MuSCs: Muscle Satellite Cells

DMD: Duchenne Muscular Dystrophy

H3K9 KMTs: Histone 3 Lysine 9 Methyltransferase

H3K9me2: Histone 3 Lysine 9 dimethylation

KMT: Histone Lysine Methyltransferase

HDAC: Histone deacetylase

HDACi: Histone deacetylase inhibitors

KD: Knock down

NL: Nuclear Lamina

LADs: Lamina-Associated Domains

CTX: Cardiotoxin

TMX: Tamoxifen

d.p.i.: Days post injury

**Sapienza, Università di Roma**  
**Ph.D. Course in Cell and Developmental Biology Cycle**

**Beatrice Biferali**

Chiara Mozzetta

**External reviewers:**

Johnny Kim

Institution: Max Planck Institute for Heart and Lung Research,  
Germany

Mail: johnny.kim@mpi-bn.mpg.de

AIT-SI-ALI Slimane

Institution: Centre National de la Recherche Scientifique CNRS –  
Université Paris Diderot, Sorbonne Paris Cité

Mail: slimane.aitsiali@univ-paris-diderot.fr

**Sommario Inglese**

Fibro-Adipogenic Progenitors (FAPs) are crucial regulators of muscle homeostasis as they possess the intrinsic ability to either support muscle regeneration or to contribute to fibro-adipogenic degeneration of dystrophic muscles. Therefore, the elucidation of the molecular mechanisms controlling their phenotypical plasticity holds therapeutic potential. Here we provide evidence that FAPs are particularly enriched in histone H3 lysine K9 methyltransferases (H3K9 KMTs), G9a, GLP and Prdm16. Our data indicate that

H3K9 KMTs safeguard FAPs identity by repressing alternative transcriptional programs through deposition of H3K9 dimethylation (H3K9me2). Specifically, we show that Prdm16 controls G9a/GLP-mediated deposition of H3K9me2 at muscle-specific loci. Of note, we found Prdm16, G9a and GLP particularly enriched at the nuclear lamina (NL) of FAPs, suggesting that they organize heterochromatin at the nuclear periphery to maintain the stable repression of genes encoding alternative developmental regulators. Accordingly, pharmacological inhibition or RNAi-mediated knock-down (KD) of H3K9 KMTs de-repress master myogenic genes in FAPs and induce the muscle differentiation program. Together, our findings reveal a FAPs-specific epigenetic axis important to control their identity. These findings are important especially for the possible therapeutic application to conceive strategies aimed to reprogram FAPs fate *in vivo* to prevent degeneration of diseased muscles.

### **Sommario Italiano**

I progenitori Fibro-Adipogenici (FAPs) sono una popolazione cellulare cruciale nel regolare l'omeostasi muscolare. I FAPs possiedono un'intrinseca capacità di supportare la rigenerazione muscolare attraverso la promozione del differenziamento delle cellule staminali muscolari, le cellule Satelliti (MuSCs); tuttavia, possiedono la capacità di differenziare esse stesse in cellule fibrotiche e adipose, contribuendo alla degenerazione del tessuto muscolare. In questo lavoro, evidenziamo che i FAPs esprimono livelli elevati di metiltrasferasi, specifiche per la mono- e la dimetilazione della Lisina (K) 9 dell'istone H3 (H3K9 KMTs), quali G9a, GLP e Prdm16. I nostri dati indicano che queste metiltrasferasi sono particolarmente arricchite alla lamina nucleare e sono in grado di salvaguardare l'identità dei FAPs reprimendo programmi

trascrizionali alternativi attraverso la deposizione di H3K9me2. In questo lavoro dimostriamo che Prdm16 controlla il reclutamento di G9a/GLP e la deposizione di H3K9me2 in specifiche regioni muscolari. Inoltre, l'inibizione farmacologica e il *knock-down* delle KMT H3K9 è in grado di attivare i principali geni miogenici nei FAPs, inducendo un'attivazione del programma di differenziamento muscolare. I nostri dati saranno utili per concepire strategie volte a riprogrammare il destino dei FAP *in vivo*, prevenendo così la degenerazione e la perdita progressiva della funzione muscolare in malattie neuromuscolari degenerative.

## **AWARDS AND GRANTS**

Recipient of Mobility Projects Fellowship for PhD students of Sapienza University of Rome-hosted for three months in Prof. Stricker's lab at Freie University of Berlin (Germany).

## **STAGES**

“Bioinformatics: Theory and application from genomes to drugs”. June 2018 at the Department of Biochemical Sciences” A. Rossi Fanelli, Sapienza University of Rome

RNAseq analysis workshop, Torino – Italy 28-31 March 2017 organizer by Bx2M (Associazione Culturale per la medicina Molecolare, Via Saorgio 105, 10147 Torino).

## **CONFERENCE ORAL PRESENTATIONS**

- Oral Presentation at “2019 Myogenesis Gordon Research Seminar” 8-9 June 2019 Renaissance Tuscany Il Ciocco

Lucca (Barga), Italy "H3K9 Methylation Controls Fibro-Adipogenic Progenitors Identity and Skeletal Muscle Repair".

- Oral Presentation at "XIII IIM-Myology Meeting " 13-16 October 2016 Assisi (PG) Italy "Role of Histone H3 lysine 9 methyltransferases During Duchenne Muscular Dystrophy progression ".

## CONFERENCE COMMUNICATIONS

- Poster Presentation at “2019 Myogenesis Gordon Research Seminary” 8-9 June 2019 Renaissance Tuscany Il Ciocco Lucca (Barga), Italy "H3K9 Methylation Controls Fibro-Adipogenic Progenitors Identity and Skeletal Muscle Repair" - **Beatrice Biferali**, V. Bianconi, R. Maggio, T. Santini, G. Peruzzi, C. Mozzetta.
- Poster Presentation at “2019 Myogenesis Gordon Research Conference” 9-14 June 2019 Renaissance Tuscany Il Ciocco Lucca (Barga), Italy "H3K9 Methylation Controls Fibro-Adipogenic Progenitors Identity and Skeletal Muscle Repair" - **Beatrice Biferali**, V. Bianconi, R. Maggio, T. Santini, G. Peruzzi, C. Mozzetta.
- Poster Presentation at “2017 Myogenesis Gordon Research Conference” 11-16 June 2017 Renaissance Tuscany Il Ciocco Lucca (Barga), Italy "Epigenetic regulation of Fibro-Adipogenic Progenitors’ plasticity during skeletal muscle regeneration and disease" - **Beatrice Biferali**, V. Bianconi, and C. Mozzetta.

## LIST OF PUBLICATIONS

- **B. Biferali**, D. Proietti, C. Mozzetta, L. Madaro (2019) “Fibro-Adipogenic Progenitors (FAPs) cross-talk in skeletal muscle: the social network”. Review *Frontiers Physiology- Striated Muscle* doi: [10.3389/fphys.2019.01074](https://doi.org/10.3389/fphys.2019.01074)
- **Biferali B.** and Mozzetta C. (2019) Chapter 13- “Skeletal muscle regeneration in physiological and pathological conditions”. Volume on “Epigenetics and Regeneration” for the series “Translational Epigenetics” Elsevier. <https://doi.org/10.1016/B978-0-12-814879-2.00013-3>
- A. Cirigliano, A. Amelina, **B. Biferali**, A. Macone, C. Mozzetta, M. M. Bianchi, M. Mori, B. Botta, E. Pink, R. Negri, T. Rinaldi. (2019) “Statins interfere with the attachment of *S.cerevisiae* mtDNA to the inner mitochondrial membrane”. *Journal of Enzyme Inhibition and Medicinal Chemistry (IENZ)* <https://doi.org/10.1080/14756366.2019.1687461>
- A. Cipriano, M. Macino, G. Buonaiuto, T. Santini, **B. Biferali**, G. Peruzzi, Alessio Colantoni, C. Mozzetta and M. Ballarino. "Epigenetic regulation of *Wnt7b* expression by the *cis*-acting long noncoding RNA *lnc-Rewind* in muscle stem cells”. *Under revision* doi: <https://doi.org/10.1101/2020.01.03.894519>
- **B. Biferali**, V. Bianconi, D. Fernandez. Perez, S. Vom Hofe-Schneider, F. Marullo, R. Maggio, T. Santini, P. Diego, F. Chiacchiera, S. Stricker, G. Peruzzi, C. Mozzetta. “H3K9 methylation controls Fibro-Adipogenic Progenitors

identity and skeletal muscle repair”. *Manuscript in preparation*

- Bianconi V., **Biferali B.**, Fernandez Perez D., Maggio R., Pasini D., Peruzzi G., Mozzetta C. “Inhibition of G9a/GLP promotes skeletal muscle regeneration and morphological recovery of dystrophic muscles”. *Manuscript in preparation*
- Publication of the abstracts presented during XIV IIM-MYOLOGY Meeting 12-15 October 2017 Assisi (PG) Italy in a special issue of the journal "European Journal of Translational Myology" – “Histone H3 Lysine 9 methyltransferases G9a and GLP as potential pharmacological targets in skeletal muscle regeneration and Duchenne Muscular Dystrophy”. Valeria Bianconi, **Biferali B.**, C. Mozzetta.
- Publication of the abstracts presented during the "XIII IIM-Myology Meeting " 13-16 October 2016 Assisi (PG) Italy in a special issue of the journal "European Journal of Translational Myology"- "Role of Histone H3 lysine 9 methyltransferases During Duchenne Muscular Dystrophy progression" – **B. Biferali**, V. Bianconi, and C. Mozzetta.
- Publication of the abstracts presented during the "XIII IIM-Myology Meeting " 13-16 October 2016 Assisi (PG) Italy and publication of abstract in the journal "European Journal of Translational Myology" entitled: " Histone H3 Lysine 9 methyltransferases G9a and GLP as potential pharmacological targets in skeletal muscle regeneration and Duchenne Muscular Dystrophy”- Valeria Bianconi, **Biferali B.**, C. Mozzetta.

## **ADDITIONAL INFORMATION (optional)**

Organizer of the 10th BeMM Symposium 2019 as PhD student for Cellular and Developmental Biology PhD Course - Rome 22/11/2019 Aula Pocchiari -Istituto Superiore di Sanità Viale Regina Elena, 299

**H3K9 methylation controls  
Fibro-Adipogenic Progenitors identity and skeletal  
muscle repair**

**PhD Student**  
Beatrice Biferali

**SHORT SYNOPSIS OF THE THESIS**

Fibro-Adipogenic Progenitors (FAPs) are crucial regulators of skeletal muscle homeostasis. FAPs have been defined as bi-potent muscle-resident progenitors capable to differentiate *in vitro* and *in vivo* in fibroblasts and adipocytes (Joe et al., 2010; Uezumi et al., 2010). In fact, during skeletal muscle regeneration, FAPs quickly proliferate and expand, prior to MuSCs, providing a transient favorable environment to promote, paracrinally, satellite cell-mediated regeneration (Heredia et al., 2013; Joe et al., 2010, Lemos et al., 2015; Lukjanenko et al., 2019, Mozzetta et al., 2013). Intriguingly, beyond their supportive role in muscle regeneration, FAPs have been shown to be the major source of fibroblasts and adipocytes in degenerating muscles (Kopinke et al., 2017; Mozzetta et al., 2013; Uezumi et al., 2010; Uezumi et al., 2011). When the regeneration fails, as in dystrophic muscles at advanced stages of disease, these cells turn into fibro-adipocytes, being no longer able to promote myogenic potential of satellite cells and leading to gradual accumulation of fatty and fibrotic infiltrate within the muscle (Kopinke et al., 2017; Mozzetta et al., 2013; Uezumi et al., 2010; Uezumi et al., 2011). This dual role of FAPs, makes them an attractive target for the development of pharmacological therapies aimed to improve regeneration, and to hinder fibro-adipogenic

degeneration, of diseased muscles (Biferali et al., 2019). Recent studies have begun to elucidate the signaling pathways responsible of FAPs phenotypical plasticity in physiological and pathological conditions (Heredia et al., 2013; Kopinke et al., 2017; Lees-Shepard et al., 2018; Lemos et al., 2015), but the epigenetic events that govern their alternative phenotypes are still rather unexplored. Therefore, the identification of the epigenetic players governing their phenotypical plasticity holds therapeutic potential. Chromatin modifying enzymes offer a repertoire of possible druggable targets. Among them, lysine methyltransferases (KMTs) are becoming increasingly studied thanks to their selectivity for defined histone residues and degree of methylation. Preliminary evidence accumulated in our laboratory, and data from the literature, led us to hypothesize that Histone H3 lysine 9 (H3K9) KMTs might act as key stabilizing factors of FAPs-specific gene expression programs possibly regulating their myo-adipogenic switch. Here, we found that Prdm16, G9a and GLP are particular enriched in FAPs, as compared to MuSCs. We show that pharmacological inhibition or RNAi-mediated knock-down (KD) of either G9a/GLP and Prdm16 de-repress master myogenic genes in FAPs and induce their myogenic differentiation. Moreover, we provide evidence that Prdm16 controls G9a/GLP-dependent H3K9me2 deposition at muscle-specific loci. We show that H3K9me2 is specifically restricted to a layer of peripheral heterochromatin in FAPs. Of note, Prdm16, G9a and GLP are enriched at the nuclear lamina, where we found confined the genomic loci of master myogenic genes, such as *MyoD*. Moreover, to define the functional role of Prdm16-dependant H3K9 methylation *in vivo*, we conditionally ablate it in FAPs generating Prdm16<sup>lox/lox</sup>:PDGFR $\alpha$ <sup>CreERT2/+</sup> double transgenic mice. We then assessed the impact of FAP-specific Prdm16 depletion in the overall muscle regeneration process and in FAPs fate determination. Finally, by taking advantage of different murine

models, comprising FAPs-specific reporter mice (PDGFR $\alpha$ -H2B:EGFP mice) and a FAP-specific lineage tracer (Osr1GCE/+;R26RmTmG/+ mice) (Vallecillo-Garcia et al., 2017; Stumm et al., 2018), we assessed the capacity of FAPs to participate to myogenesis *in vivo*, by treating them with the G9a/GLP specific inhibitor (A-366). In conclusion, we demonstrate that inhibition of Prdm16-G9a/GLP pathway promotes FAPs participation to myogenesis upon induction of skeletal muscle regeneration. Taken together our data identified a FAPs-specific epigenetic axis critical to maintain the stable silencing of the myogenic program. Notably, we demonstrate that this repression can be reverted by the use of H3K9 KMTs specific inhibitors to reprogram FAPs towards myogenesis, leading to an overall acceleration of the muscle regeneration process. Indeed, the acquisition of the myogenic differentiation capacity upon inhibition of Prdm16/G9a/GLP is accompanied by a decreased adipogenic differentiation, which is in line with previous studies reporting that these two differentiation programs are mutually exclusive to guarantee robustness and discreteness of cell fates (Sunadome et al., 2014). This evidence also suggests that strategies aimed to inhibit G9a/GLP activity might represent a way to reprogram FAPs fate towards myogenesis, thus blocking their adipogenic degeneration, with obvious beneficial implications in the context of muscle degenerative diseases characterized by fatty and fibrotic infiltrations, such as Duchenne Muscular Dystrophies (DMD).